Yekaterina Pokhilchuk, B.Sc.

Statin Side Chain Synthesis via Whole-Cell Biocatalysis in Continuous Flow

MASTER'S THESIS

to achieve the university degree of

Diplom-Ingenieur

Master's degree programme: Chemical and Pharmaceutical Engineering

submitted to

Graz University of Technology

Supervisor

Assoc. Prof. DI Dr. techn. Heidrun Gruber-Wölfler

Institute of Process and Particle Engineering

Graz, October, 2019

AFFIDAVIT

I declare that I have authored this thesis independently, that I have not used other than the declared sources/resources, and that I have explicitly indicated all material which has been quoted either literally or by content from the sources used. The text document uploaded to TUGRAZonline is identical to the present master's thesis.

_____	_____
Date	Signature

Abstract

Statins are the most effective and widely prescribed drugs for lowering cholesterol levels in patients with coronary artery disease (CAD), a leading cause of death worldwide. Their activity is attributed to the chiral lateral chain that requires high chemical and stereochemical purity. Biocatalysis provides the necessary tools for safe stereoselective synthesis with minimized chemical waste. Furthermore, continuous processes are a promising avenue researched by and applied at the pharmaceutical industry for its cost and energy efficient way of continuously supplying a required product. This work presents a whole-cell biocatalysis approach applied in continuous flow for synthesis of a statin lateral chain precursor catalyzed by a deoxyribose-5-phosphate aldolase (DERA) mutant (C47M).

Acetaldehyde, chloroacetaldehyde, acrolein, benzaldehyde, and cinnamaldehyde were screened in batch for their potential to act as acceptor molecules in a DERA-catalyzed sequential aldol addition reaction. The substrate that performed the best was further applied for the optimization and evaluation of statin side chain synthesis in continuous flow. The enzyme enclosed in lyophilized *E.coli* cells was entrapped in a sodium alginate gel matrix and immobilized on a luffa sponge by cross-linking the gel matrix onto the sponge. The alginate-loofa matrix (ALM) was packed into an HPLC column and tested with the chosen aldehyde substrate with different process parameters. The results were evaluated to assist the feasibility of a DERA-catalyzed statin lateral chain precursor synthesis in continuous flow.

Chloroacetaldehyde was chosen as an acceptor molecule for the continuous flow experiments. The optimum conditions while using the HPLC column were determined to be 0.5 M acetaldehyde and 0.25 M chloroacetaldehyde substrate concentration, 0.1 mL/min flowrate, and 32.5 °C reaction temperature. The results demonstrated that a DERA-catalyzed sequential aldol addition reaction completed in continuous flow is a promising avenue for the statin side chain synthesis. However, the immobilization technique requires further improvement due to the observed enzyme leaching.

Kurzfassung

Statine sind die effizientesten und am häufigsten verschriebenen Arzneistoffe zur Senkung des Blut-Cholesterinspiegels bei Patienten mit Herz-Kreislauf-Erkrankungen (HKL-Erkrankungen), eine der häufigsten Todesursachen weltweit. Hohe Enantiomerenreinheit der chiralen Seitenkette und chemische Reinheit des gesamten Wirkstoffmoleküls sind entscheidend für die physiologische Wirkung der Statine. Biokatalyse bietet alle notwendigen Werkzeuge für die stereoselective Synthese bei minimalem Anfall an chemischem Müll. In der pharmazeutischen Industrie sind zudem Entwicklung und Anwendung kontinuierlicher Prozesse ein vielversprechender Ansatz, um die kontinuierliche Bereitstellung des gewünschten Produkts kosten- und energieeffizient zu garantieren. Diese Arbeit präsentiert die Anwendung eines Deoxyribose-5-phosphate Aldolase (DERA) Mutanten (C47M) in Ganzzellbiokatalyse im kontinuierlichen Durchflussreaktor zur Synthese einer Vorstufe der Statin-Seitenkette.

Acetaldehyd, Chloroacetaldehyd, Acrolein, Benzaldehyd und Zimtaldehyd wurden im Batch auf ihre Potenzial als Akzeptormolekül in der DERA-katalysierten sequenziellen Aldol-Addition zu dienen, getestet. Jenes Substrat, welches die besten Ergebnisse lieferte, wurde anschließend für die Optimierung und Evaluierung der Synthese der Statin-Seitenkette im kontinuierlichen Durchflussreaktor verwendet. Das Enzym in lyophilisierten *E.coli* Zellen wurde mit einer Natrium-Alginat Gelmatrix durch Vernetzung auf Luffa Schwamm immobilisiert. Diese Alginate-Luffa Matrix (ALM) wurde in eine HPLC-Säule gepackt und mit dem gewählten Aldehyd unter verschiedenen Prozessbedingungen getestet. Die Ergebnisse wurden dahingehend evaluiert, die Machbarkeit einer DERA-katalysierten Synthese der Vorstufe der Statin-Seitenkette im kontinuierlichen Durchflussreaktor zu beweisen.

Chloroacetaldehyd diente als Akzeptormolekül für die kontinuierlichen Versuche. Die optimalen Reaktionsbedingungen in der HPLC-Säule wurden ermittelt und liegen bei einer Substratkonzentrationen von 0.5 M Acetaldehyd und 0.25 M Chloroacetaldehyd, einer Durchflussrate von 0.1 mL/min und einer Temperatur von 32.5 °C. Die Ergebnisse zeigen, dass die DERA-katalysierte sequentielle Aldol-Addition im kontinuierlichen Durchflussreaktor einen vielversprechenden Ansatz für die Synthese der Statin-Seitenkette darstellt. Jedoch bedarf

es Verbesserungen in der Immobilisierungsmethode, um das Auswaschen des Enzymes aus der Matrix zu minimieren.

Acknowledgement

I would like to express appreciation to all the people who supported me throughout my journey to completion of the master's degree and acknowledge them below:

First, I would like to thank my supervisor Assoc. Prof. DI Dr. techn. Heidrun Gruber-Wölfler for giving me the opportunity to pursue my master's thesis in your laboratory and for the guidance. Thanks as well to my secondary supervisor Bianca Grabner, M.Sc. You were always available to answer my countless questions. I am especially thankful for your patience. It was a long and rocky road to the defense and you have supported me along the way. I would like to thank the CoSy Bros, especially Manuel Maier. Thank you for being there when I needed help and I am not sure I can survive in Canada without your delicious honey wine.

Words cannot describe how grateful I am for my friends and family. Maddie DeWinter and Lea Sorret, thank you so much for all the fun trips we had and all the support you provided. Maddie, thank you as well for proofreading my thesis despite your busy schedule. I would also like to thank Alona Starykovska for all the chocolate, singing, and late-night talks. Thank you for always supporting me and helping me through the rough patches. Thanks as well to Taylor Burton, my best friend who has an incredible amount of patience and loves me for who I am. I am especially thankful to Roman Matskiv. Your immense support, love, and encouragement have pushed me forward and I could not have done this without you being by my side.

Contents

List of Figures

List of Tables

List of Symbols

Symbol	Definition
c	Concentration [mol/L]
D	Longitudinal dispersion coefficient [m^2/s]
E	Exit age distribution [s^{-1}]
F	Cumulative age distribution [-]
L	Length [m]
t	Time [min]
$\bar{t}$	Mean residence time [min]
$\bar{t}_{exp}$	Experimental mean residence time [min]
$\bar{t}_{th}$	Theoretical mean residence time [min]
u	Superficial velocity [m/s]
v	Flow rate [mL/min]
V_R	Reactor volume [mL]
V_S	Sponge volume [mL]
ρ	Density [g/mL]
σ^2	Variance [s^2]

Abbreviations

Abbreviation	Definition
AA	Acetaldehyde
AAPS	American Association of Pharmaceutical Scientists
ALM	Alginate-loofa matrix
API	Active pharmaceutical ingredient
CAA	Chloroacetaldehyde
CAD	Coronary artery disease
C-C	Carbon-carbon
CDER	Center for Drug Evaluation and Research
CM	Continuous manufacturing
CSTR	Continuous stirred tank reactor
CVD	Cardiovascular disease
de	Diastereomeric excess
DERA	2-deoxy-D-ribose-5-phosphate aldolase
DHAP	Dihydroxyacetone phosphate
DMSO	Dimethyl sulfoxide
DoE	Design of experiments
ee	Enantiomeric excess
E. coli	Escherichia coli
EMA	European Medicines Agency
EtOAc	Ethyl acetate
EtOH	Ethanol

Abbreviation	Definition
FDA	Food and Drug Administration
FID	Flame ionization detector
GC	Gas chromatography
HMG	3-hydroxy-3-methylglutaryl
HMG-CoA	3-hydroxy-3-methylglutaryl-coenzyme A
HPLC	High-performance liquid chromatography
ID	Inner diameter
IPTG	Isopropyl β-D-1-thiogalactopyranoside
LB	Lysogeny broth (Luria broth)
LDL	Low-density lipoproteins
LDL-C	Low-density lipoproteins cholesterol
MeCN	Acetonitrile
MeOH	Methanol
NaCl	Sodium chloride
NMR	Nuclear Magnetic Resonance
OD	Optical density
ONC	Overnight culture
PBR	Packed bed reactor
RP-HPLC	Reversed phase high-performance liquid chromatography
Rpm	Revolutions per minute
RTD	Residence time distribution
SA	Synthetic air
SDS-PAGE	Sodium dodecyl sulfate-polyacrylamide gel electrophoresis
TB	Terrific broth

Abbreviation	Definition
TEOA	Triethanolamine
TIM	Triosephosphate Isomerase
TU	Technical University
U.S.	United States
UV-vis	Ultraviolet and visible
WT	Wildtype

1 Introduction

Cardiovascular disease (CVD) is a group of diseases involving heart and arteries that cause significant global morbidity and mortality and have been the leading cause of death in the world for the last 18 years [1]. In 2016, CVD was responsible for 17.9 million deaths, or 31 % of all deaths worldwide [2]. Due to CVD's widespread detrimental impact on global health, there remains significant potential for effective and affordable treatment to improve disease outcomes.

The primary cause of death among CVD patients is coronary artery disease (CAD) [1]. CAD is characterized by artherosclerosis – a buildup of plaque in the arteries of the heart that partially occludes the arteries and therefore reduces the supply of the oxygen to the heart [3]. One of the main risk factors for developing CAD is elevated blood cholesterol due to its crucial role in the formation of arterial plaques [4]. Cholesterol is transported into the circulatory system by different types of lipoproteins, however, the majority of transported cholesterol is attributed to the low-density lipoproteins (LDL) [5]. Arterial plaque formation is accredited to an increased plasma concentration of low-density lipoprotein cholesterol (LDL-C), making LDL-C a primary CAD drug target.

Statins are the most commonly used medication to lower LDL-C levels in the blood. They are competitive inhibitors of HMG-CoA reductase (3-hydroxy-3-methylglutaryl-coenzyme A reductase), an enzyme that catalyzes a rate-limiting step in cholesterol biosynthesis. HMG-CoA reductase inhibition decreases cholesterol production and lowers its levels in the blood. One of the most prevalent statins is atorvastatin (Lipitor), synthesized by Pfizer since 1996 [6]. It is known as the best-selling blockbuster drug of all time [6]. In 2019, an additional statin, atorvastatin, placed 3rd in the most prescribed medications in the U.S.; therefore, statins represent a significant share of the pharmaceutical market [7].

Synthesis of statins is a very challenging task due to the necessity of high chemical and stereochemical purity for adequate activity [6], [8], [9]. The pharmaceutical industry has addressed this issue by investigating biocatalytic routes for stereoselective synthesis of statin building blocks. Biocatalysis offers an attractive approach for stereoselective synthesis of chiral molecules under mild conditions [9]. A substantial amount of attention has been given to aldolases, biocatalysts that

are capable of sequential aldol reactions yielding a product with multiple chiral centers. 2-deoxyribose-5-phosphate aldolase (DERA) is of particular interest for statin side chain synthesis due to its ability to sequentially accept three aldehydes with high stereoselectivity [10]. This two-step process with simple and inexpensive raw materials yields a lactol type derivative that can be easily oxidized to form lactonized statin side chains with the desired stereochemistry [6]. Therefore, DERA is a promising solution for the challenging chiral side chain synthesis of statins.

However, DERA application in pharmaceutical industry presents its own obstacles, including long reaction times, high enzyme load, and difficult scale up [6]. Additionally, the vast majority of pharmaceutical drug products, including statins, are manufactured in a batch mode. Despite the dominance of batch manufacturing in pharmaceutical industry, batch-based approach often results in long production times and inconsistent product quality [11]. An alternative approach to the traditional batch process is continuous manufacturing (CM) that has been receiving more attention by academic research and industry for pharmaceutical implementations [11], [12]. CM provides a variety of benefits, including a reduction of manufacturing time, constant product quality, agility, and reduced scale-up efforts [13]. These benefits address, and potentially resolve, the above mentioned bottlenecks of DERA-catalyzed step of statin synthesis in batch.

In order to apply an enzymatic step in a continuous process, enzymes can be fixed in the reactor throughout the reaction. Immobilization of enzyme on an inert material is a simple way to secure the enzyme. This approach simplifies batch to continuous transformation while providing additional benefit of enzyme stability [14], [15].

The focus of this master's thesis was to investigate the DERA-catalyzed step in statin side chain synthesis and its potential to be performed as a continuous process. Five different substrates were screened in batch and the enzyme was immobilized on a loofa sponge solid support. The optimal substrate and the immobilized enzyme were analyzed in flow to determine continuous process parameters. The obtained results were evaluated for the feasibility of an in-flow DERA-catalyzed step in statin side chain synthesis.

2 Theoretical Background

2.1 Statins

Statins are important lipid lowering drugs prescribed throughout the world [8], [16]. These small molecules are effective therapeutics used for primary and secondary prevention of CAD and are essential in lowering risk of CVD [5], [8], [16], [17]. Statins were discovered in 1973 by Dr. Akira Endo, who, together with Dr. Masao Kuroda, isolated the first statin, mevastatin, from *Penicillium citrinum*, a fungus that infects citrus fruits [18], [19]. Mevastatin was never marketed but it played a crucial role in the development of the first commercially available statin, lovastatin, which was isolated from the fungus *Aspergillus terreus* by Merck in 1976 [18]. Lovastatin was approved by the Food and Drug Administration (FDA) for medical use in 1987 [17], [18].

Statins lower LDL-C levels by competitively inhibiting HMG-CoA reductase in the liver. HMG-CoA reductase catalyzes the rate-limiting step of the hepatic cholesterol synthesis pathway and irreversibly reduces HMG-CoA to form mevalonate. Mevalonate is the initial reactant for isopentenyl pyrophosphate synthesis – a key building block of cholesterol [5], [20]. A simplified reaction scheme of this process is presented in Figure 2.1.
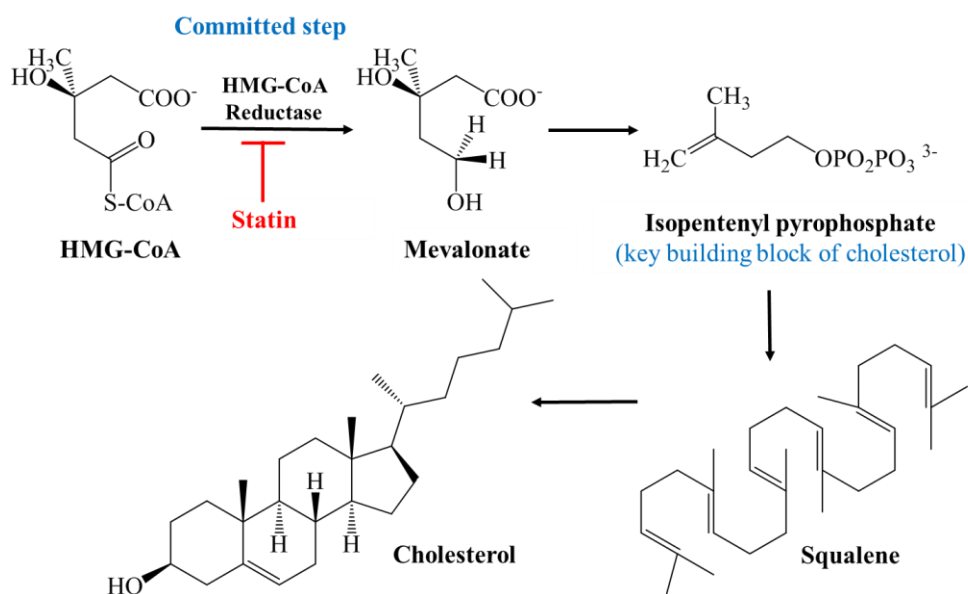
Figure 2.1: Simplified reaction scheme of cholesterol synthesis and statin mechanism of action [20].

In order to improve pharmacokinetics and efficacy of natural statins, semi-synthetic and fully synthetic statins were developed and now dominate the market. Natural and semi-synthetic statins are frequently referred to as type 1 statins, and fully synthetic statins, also known as super-statins, are classified as type 2. Statins consist of a hydrophobic core covalently linked to a lateral chain with an HMG moiety [6], [21]. The structural similarity of statins and HMG-CoA is responsible for statins' antagonistic activity. Most of the natural and semi-synthetic statins have side chains in a form of a lactone that is hydrolyzed *in vivo* to the active hydroxyl-acid, whereas lateral chains of super-statins are initially in their active form of dihydroxy heptenoic or heptanoic acid [8], [21]. Common statin structures are illustrated in Figure 2.2.
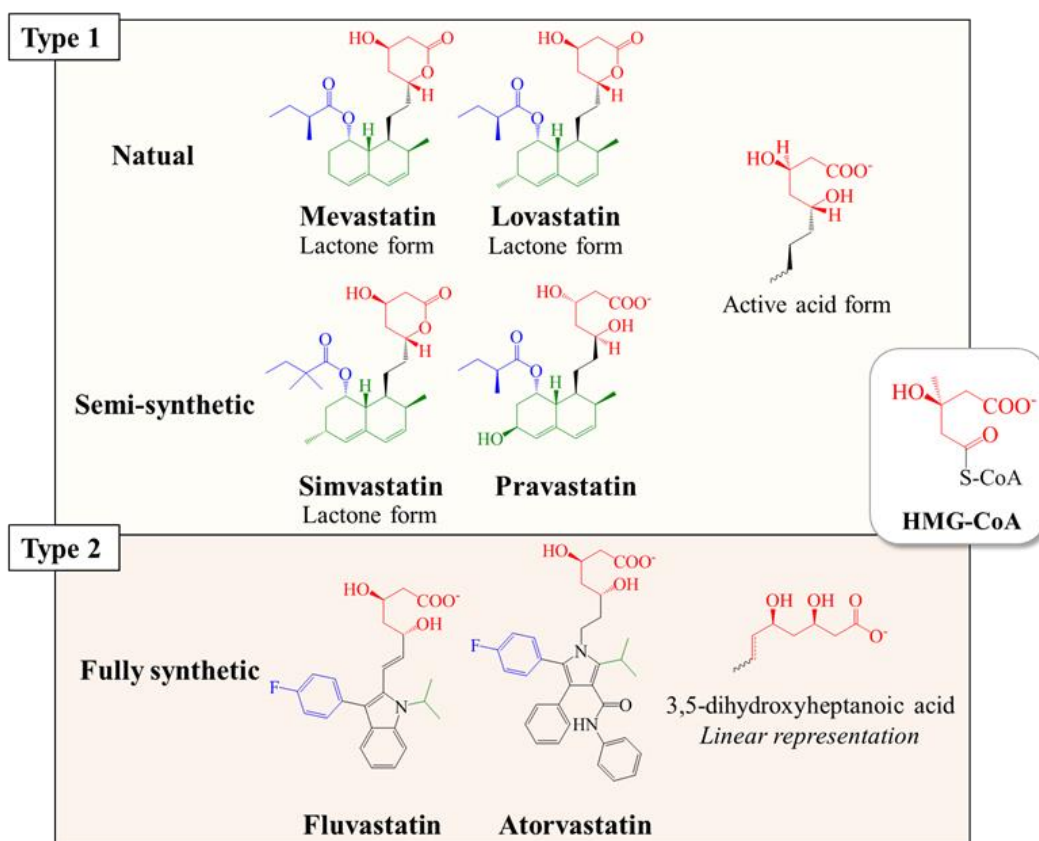
Figure 2.2: Structures of HMG-CoA and selected type 1 and type 2 statins. The HMG moiety is labeled in red. Butyryl groups and fluorophenyl groups are indicated in blue. Decalin rings and propyl groups are indicated in green. The HMG moiety in type 2 statins is also shown in a linear form [21].

The central core of type 1 statins consists of a substituted chiral decalin ring with a butyryl group. Type 2 statin cores are heterocyclic aromatic rings with a fluorophenyl group and a propyl group attached to a central ring of the core [8], [21]. The butyryl group of type 1 statins and fluorophenyl group of type 2 stains occupy a similar region of the HMG-CoA reductase upon binding and are

marked in blue in Figure 2.2. The substituted decalin rings of type 1 statins and the propyl group of type 2 statins have the same functionality in the molecule and are marked in green in Figure 2.2.

A statin's chiral lateral chain functions as a pharmacophore of the molecule responsible for its pharmacokinetic and pharmacodynamic characteristics. Chiral substances have different physiochemical and biochemical properties and thus cause different pharmacologic or toxicological effects [22], [23]. Only one enantiomer of statin is active and the final drug product requires high stereochemical purity (> 99.5% enantiomeric excess, ee, > 99% diastereomeric excess, de) for adequate activity, which is a significant challenge in manufacturing [8], [24]. Additionally, full characterization of stereochemistry is mandated for market approval by several regulatory agencies, including the U.S. Food and Drug Administration (FDA) and the European Medicines Agency (EMA) [25]. The final statin drug product must be either (*3R,5R*)- or (*3R,5S*)-dihydroxyhepta(e)noic acid in order to possess the inhibitory activity (Figure 2.3). The enantiomeric configuration is dictated by the molecular structure of a statin. For instance, commonly prescribed atorvastatin is a (*3R,5R*)-enantiomer, whereas rosuvastatin is a (*3R,5S*)-enantiomer [26].
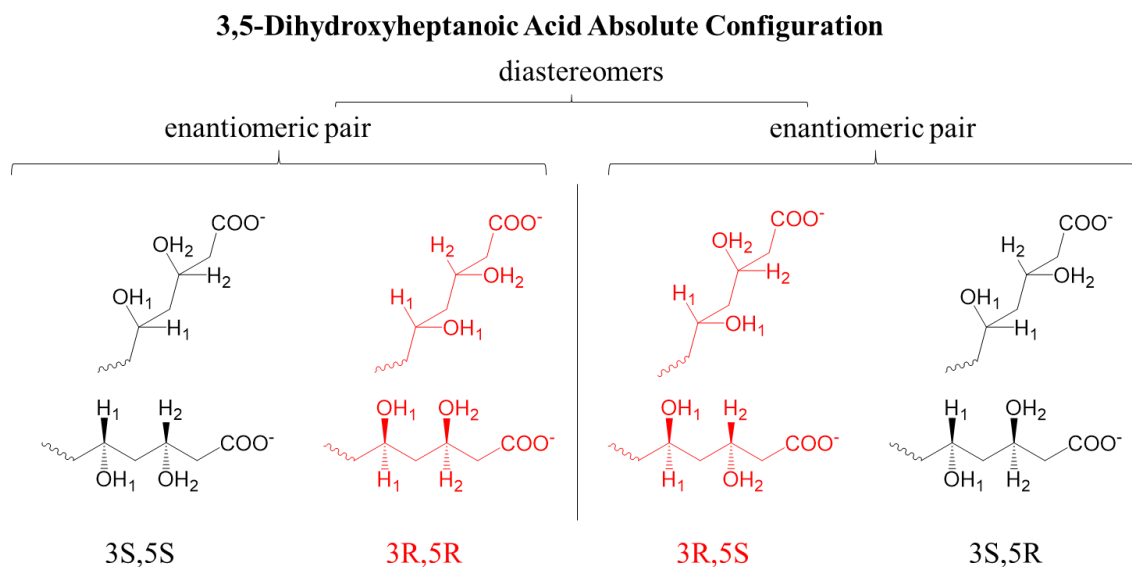
Figure 2.3: Absolute configuration of 3,5-dihydroxyheptanoic acid. The active enantiomers are indicated in red. Only one enantiomer is active per statin structure.

Several different multistep synthetic approaches have been established in industry for statin synthesis and assembly that yield optically active and pure statin molecules. However, these approaches are complex and require use of toxic and hazardous substances, include protection and

deprotection steps that increase production time, and produce chemical waste [6], [8]. An alternative approach to the established industrial statin synthesis is an implementation of a chemoenzymatic route. This approach can minimize, or even eliminate, the negative aspects of synthetic preparation of statins while producing optically pure molecule and thus, biocatalysis of statin lateral chains have been explored by pharmaceutical companies [24], [27].

2.2 Aldol Reaction

The aldol reaction is central to organic chemistry because it forms a new carbon-carbon (C-C) bond introducing two adjacent chiral centers to the product [28], [29]. The C-C bond is important because it is one of the strongest covalent bonds in *in vitro* and *in vivo* environments [30]. The strength of the covalent bond affects drug stability in formulations and drug's lifetime *in vivo* [30]. The stereochemistry affects drug's activity and was discussed above. This makes C-C bond essential for developing pharmaceuticals, agrochemicals, and new generations of other designed organic materials [31]. Thus, aldol reaction attracted chemists for statin side chain synthesis application.

In an aldol reaction, two carbonyl compounds form β-hydroxy carbonyl molecule (aldol) by nucleophilic addition, as demonstrated in Figure 2.4. If the reaction proceeds under basic conditions, a nucleophilic enolate (electron donor) is formed and attacks an electrophilic carbonyl (electron acceptor) [24]. The generated aldol product can undergo dehydration from a subsequent aldol condensation reaction (elimination).
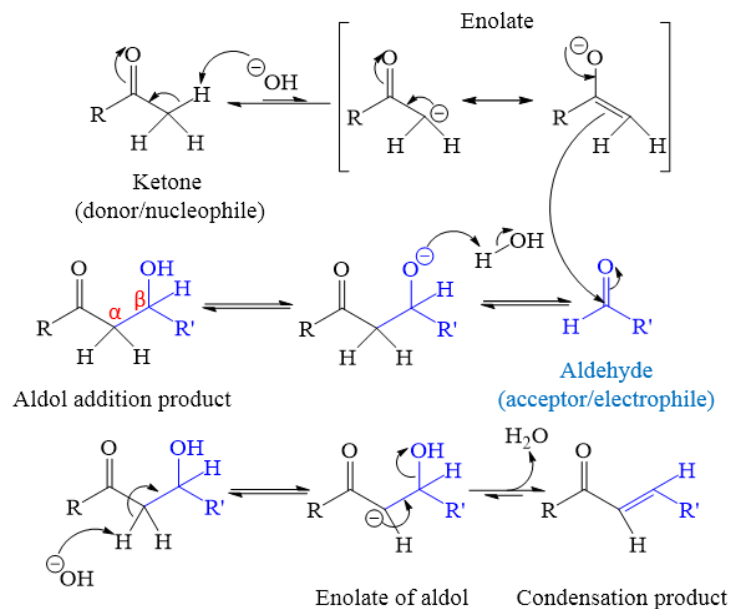
Figure 2.4: General aldol reaction mechanism between ketone and aldehyde under basic conditions showing addition and condensation products [24].

Even though the aldol reaction is a well-known reaction in organic chemistry, it has certain selectivity related drawbacks. A condensation reaction produces an undesired product for asymmetric synthesis and its formation must be avoided. Additionally, both of the carbonyl substrates can potentially act as a donor and as an acceptor, leading to self aldol and cross aldol reactions, forming four possible products, as illustrated in Figure 2.5.
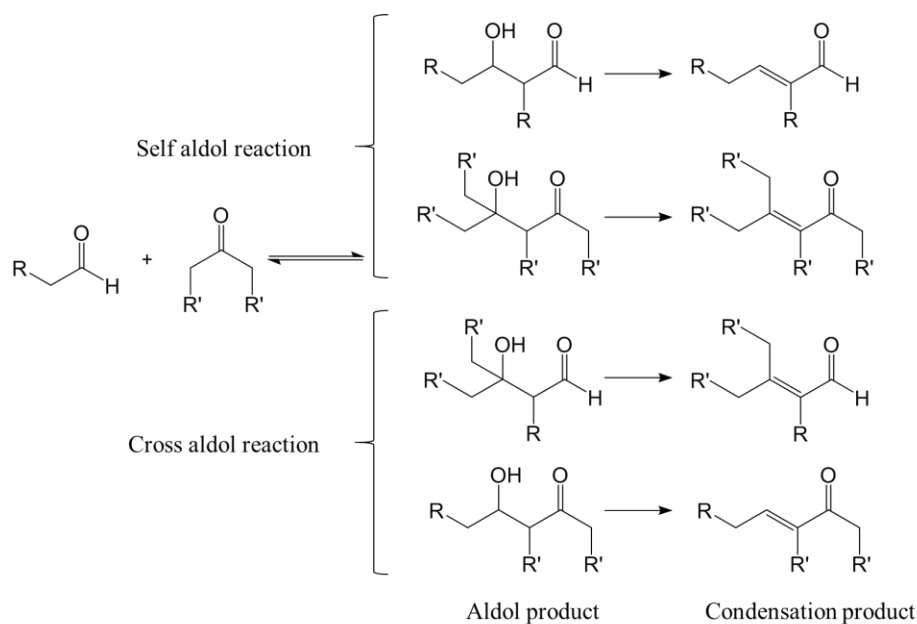
Figure 2.5: Possible aldol addition and condensation products of self aldol and cross aldol reactions [32].

Chemical aldol reactions require the use of protection/deprotection steps to improve selectivity, however, they often still result in formation of multiple by-products and generate waste [24], [33]. One way to resolve these issues is to implement enzymes in the process [32], [34].

2.3 Biocatalysts

2.3.1 General Overview

Enzymes are highly selective proteins that accelerate, or catalyze, reactions in living organisms by lowering the activation energy required to allow the reaction to progress. Activation energy can be manipulated in several ways [35]:

- Changing substrates spatial orientation to favor bond breaking/formation
- Applying mechanical stress on substrate bonds to aid in breaking
- Providing favorable microenvironment for the substrate conversion
- Transferring or accepting functional groups or protons/electrons for the substrate conversion

The enzyme-catalyzed reaction can be generally described as follows:

$$E+S \leftrightharpoons ES \leftrightharpoons EP \leftrightharpoons E+P$$
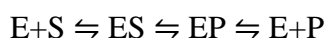
where substrate (S) binds to the active site of the enzyme (E) forming an enzyme-substrate complex (ES). After reaction completion, enzyme-product complex (EP) is formed, followed by product (P) dissociation from the enzyme to allow the enzyme to catalyze another reaction. The enzyme will not induce binding-required conformational changes for other molecules due to its high substrate selectivity [36].

Biocatalysis is a biotransformation process of substrates in chemical reactions achieved by either isolated enzymes or whole cells that contain the desired enzyme or enzyme system [37]. The enzymes used for biocatalytic reactions are frequently referred to as biocatalysts. The primary advantages and disadvantages between the two forms of biocatalysts are summarized in Table 2.1.

Table 2.1: Comparison of general advantages and disadvantages of isolated enzymes and whole cells [37], [38].

Isolated enzymes (Pure enzymes)		Whole cells (enzyme or enzyme system inside cells)	
Advantages	**Disadvantages**	**Advantages**	**Disadvantages**
• Higher reactant specificity • Better tolerance for co-solvents	• Not-suitable for multi-enzymatic reactions (complex) • Cofactor addition	• Simplicity of handling • Minimal activity loss (cell membrane protection) • Suitable for multi-enzymatic reactions	• Substrate/product inhibition • Metabolic by-product formation • Cell membrane is a mass transport barrier

Biocatalysts are widely applied in asymmetric synthesis due to their high substrate and reaction specificity and their ability to produce optically pure compounds. They are produced from renewable raw materials and require mild reaction conditions (ambient temperature and pressure, neutral pH). The generated waste from the completed biotransformation processes is biodegradable [37], [38]. Implementing biocatalysis into the production processes improves product quality, sustainability, and energy efficiency of manufacturing. Therefore, biocatalysts are an attractive approach for synthesis of chiral active pharmaceutical ingredients (API) such as statins.

Although there are many advantages to biocatalysts, there are also several drawbacks. The main disadvantages and complications include but not limited to long reaction times, difficulty of scale up, and high substrate loading [39]. Different biocatalysts, such as dehydrogenases, nitrilases, lipases, esterases, and aldolases have being investigated to mitigate these adverse attributes [6], [24]. One of the most prominent and efficient utilization of aldolases reported in the literature involves a 2-deoxy-D-ribose-5-phosphate aldolase (DERA) that produces a precursor of dihydroxy heptanoic acid with both chiral centers and the desired stereochemistry from inexpensive and commercially available starting materials in one aldol reaction step. Biocatalytic methods utilizing DERA are described in reviews by Hoyos et al. and Liljeblad et al. [6], [24].

2.3.2 Aldolases

Aldolases are a group of enzymes that catalyze aldol reactions and are classified according to their accepted donor molecules and catalytic mechanisms [32], [34], [40]–[42]. The four known donor groups are dihydroxyacetone phosphate (DHAP), pyruvate, glycine, and acetaldehyde

[32]-[34], [41], [42]. If an aldolase belongs to a DHAP-dependent group it can only activate DHAP as a donor molecule. The mechanism based aldolase are divided into two classes [33], [34], [41]. Class 1 aldolases catalyze the reaction by forming a Schiff base intermediate between the lysine residue in the active site and the donor carbonyl substrate. The general structure of a Schiff base is R2C=NR', where R'≠ H. The imine converts into its isomer enamine and attacks the acceptor carbonyl, followed by product release due to imine hydrolysis [32], [33], [42]. Class 1 aldolase general reaction mechanism is demonstrated in Figure 2.6 below. Class 2 aldolases have a metal co-factor that acts as a Lewis base upon donor substrate binding. The metal ion is bound to a histidine residue of the active site [32], [33], [42].
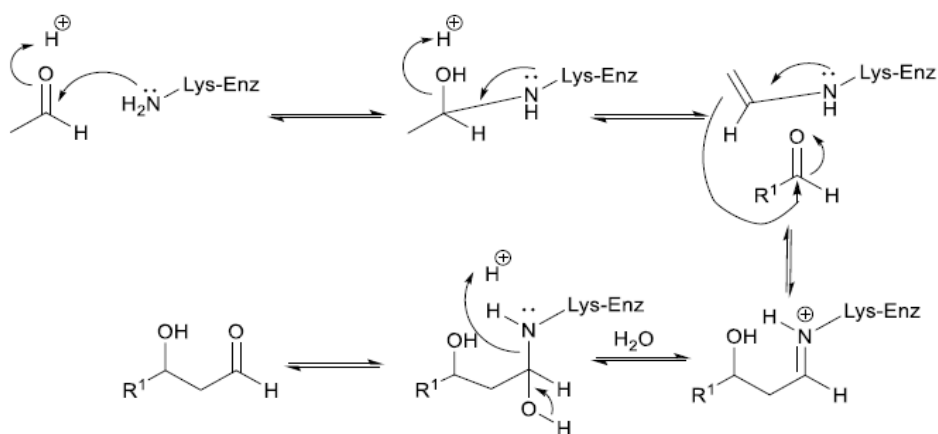
Figure 2.6: Class 1 aldolase general reaction mechanism [32].

Most *in vivo* reactions catalyzed by aldolases are related to sugar metabolism [32], [33], [43]. These enzymes have good control over cross coupling and are selective over their donor, while accepting a variety of acceptor molecules [33], [34]. A number of different aldolases are known and many are still being discovered. However, one particular aldolase – DERA – has gained attention in the biocatalysis of statins.

2.3.3 DERA (2-deoxy-D-ribose-5-phosphate aldolase)

DERA belongs to the aldehyde-dependent class 1 aldolases and can accept two aldehydes, glyceraldehyde 3-phosphate and acetaldehyde, as substrates for an aldol reaction [33], [40]. It is the only known enzyme that catalyzes reversible sequential aldol reaction using aldehydes as both donor and acceptor [33], [34], [40].The first application of DERA from a recombinant *E.coli* strain for sequentially catalyzed aldol reaction was reported by Wong et al. in 1995 [40]. The method

introduced a simple approach for preparing chiral synthons with the desired stereochemistry using inexpensive raw materials and was further applied for synthesis of statin side chain precursors. Since then, the method has been substantially optimized for potential industrial applications.

The DERA-catalyzed sequential aldol addition reaction produces a lactol-type intermediate with high stereospecificity. The intermediate is then oxidized to a lactone. The obtained lactone molecule is a precursor of the statin side chain and requires lactone ring opening to resemble the HMG moiety. This is usually a multi-step process involving protection/deprotection reactions [6]. Statin side chain synthesis starting from the DERA-catalyzed step is demonstrated below in Figure 2.7 using chloroacetaldehyde (CAA) as acceptor and acetaldehyde (AA) as donor.
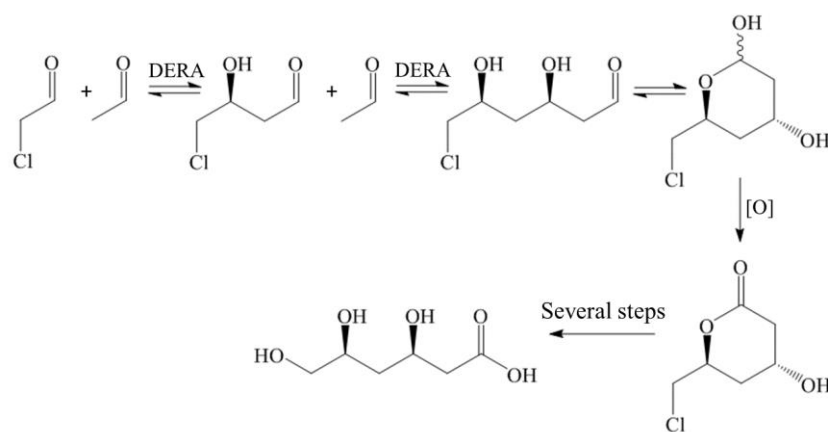
Figure 2.7: Simplified DERA-catalyzed synthesis of statin chiral building blocks from AA and CAA starting materials [6].

The active site of the wildtype DERA (DERA$_{WT}$) was studied intensively to improve its catalytic properties. The overall structure of the enzyme's catalytic domain is a TIM (Triosephosphate Isomerase) barrel $(\alpha/\beta)_8$ fold with an additional helix located after $\beta 1$ strand, as shown in Figure 2.8 (a) [44], [45]. The TIM barrel has eight α-helices on the outer lining and eight β-strands on the inner lining alternating along the peptide backbone [46]. The inner lining of eight β-strands contain the catalytically active residues [46]. The most prominent active residues found are lysine 167 (K167), lysine 201 (K201), and aspartate 102 (D102) [44], [45]. The conserved active-site water molecule (WAT29) also plays a crucial role in the catalysis [44], [45]. The stereoview of the active site residues is shown in Figure 2.8 (b).

A simplified catalytic mechanism of DERA includes (1) nucleophilic attack of K167 on donor electrophilic carbon, which initiates the Schiff base intermediate formation; (2) active-site water molecule activation. K201 and D102 residues activate WAT29 for the proton-relay (controlled movement of protons during catalysis); (3) Schiff base intermediate formation mediated by the proton-relay. The main mechanism of catalysis is the formation of the K167-donor complex, as shown in Figure 2.6; (4) attack of the formed enamine tautomer on acceptor aldehyde mediated by the proton-relay; (5) product release due to imine hydrolysis [44], [45].
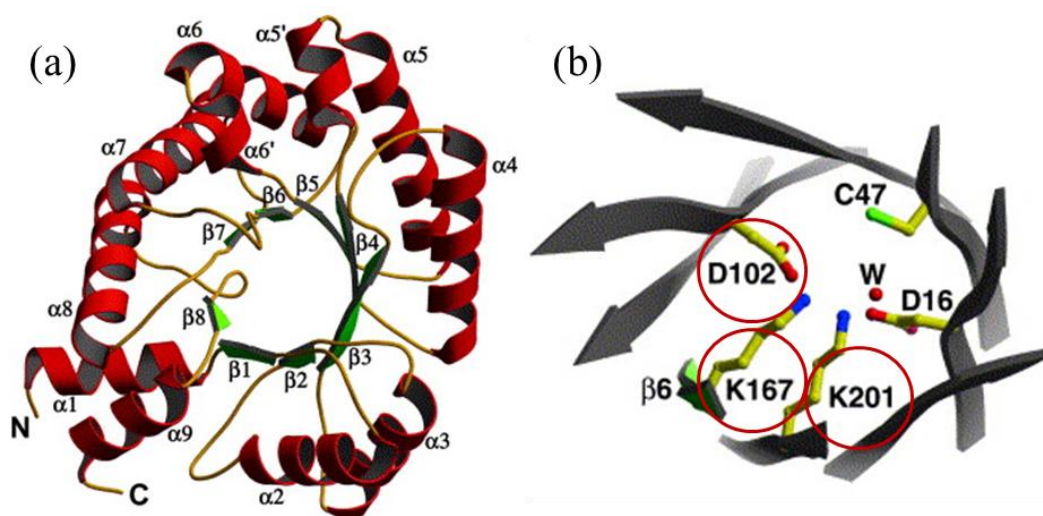
Figure 2.8: (a) DERA$_{WT}$ crystal structure ribbon diagram view. α-helices are shown in red and β-strands are shown in green [44]; (b) A stereoview of DERA$_{WT}$ active site. Most prominent active residues are circled. W represents the conserved water molecule [44].

In order to enhance the catalytic process, some scientists searched for new enzyme variants, while others attempted to modify the wildtype protein. DERA$_{WT}$ demonstrated its preference towards substrates with phosphate groups and the first modification was made to address this enzyme substrate specificity. DeSantis et al. improved DERA activity towards phosphate-free substrates by structure-based mutagenesis [47]. They have identified the phosphate bonding pocket residue that directly forms a hydrogen bond with the phosphate moiety of the substrate. The serine residue at position 238 was responsible for the hydrogen bond and was replaced by aspartate in the new DERA mutant S238D [47]. The results of the experiments were satisfactory; however, DERA still presented challenges in a form of long reaction times (several days), enzyme inhibition by CAA and AA, and high catalyst load requirement [24], [27], [28], [48]. Moreover, these problems created complications with scaling the reaction process for industrial manufacturing.

The reaction time can be significantly reduced with increased substrate concentration. However, the substrate concentration required for efficient lactol production is above enzyme's threshold and actually leads to enzyme inhibition. Enzyme inhibition by high substrate concentration was addressed in several ways, one of which is adjustment of the manufacturing process. A typical batch reaction has all of the substrates charged to the reactor simultaneously and immediately leads to high substrate concentration and enzyme inhibition. Switching to a fed-batch process enables substrate flow to the ongoing reaction thus leaving smaller substrate concentration available in the reactor and at the enzyme's active site at any point in time [27], [49]. The fed-batch process approach was implemented with different DERA variants and proved to be an efficient biocatalytic process improvement.

Substrate inhibition of DERA was also addressed by employing new co-expression strategies and screening genomic libraries from environmental DNA [10], [24], [27], [50]. Several modified enzyme variants and DERA from unknown organisms were identified and demonstrated higher CAA tolerance compared to the wildtype enzyme [27], [51]. The volumetric productivity of lactol was increased in all cases and the required enzyme load was significantly reduced [27], [51]. These experiments have targeted the CAA specific inhibition, however, in addition to CAA, AA also decreased enzyme stability and eventually deactivated it [32], [48], [52]. AA resistance was addressed by Dick et al. by analyzing mechanism-based AA inhibition of DERA [48].

Despite DERA's high control of cross reactions shown in Figure 2.5, self aldol reactions may still occur during the catalytic process. This leads to the formation of multiple side products, including crotonaldehyde, a mechanism-based inhibitor of DERA [48]. Crotonaldehyde is a product of an aldol condensation side reaction between two AA molecules. It was proposed to covalently link lysine residue (K167) of the active site to a nearby cysteine at position 47 (C47) [48]. The covalently linked K167 and C47 residues block the active site and inhibit the enzyme. The DERA-catalyzed reactions forming a key statin side chain intermediate lactol and associated side products, including crotonaldehyde, are presented in Figure 2.9.
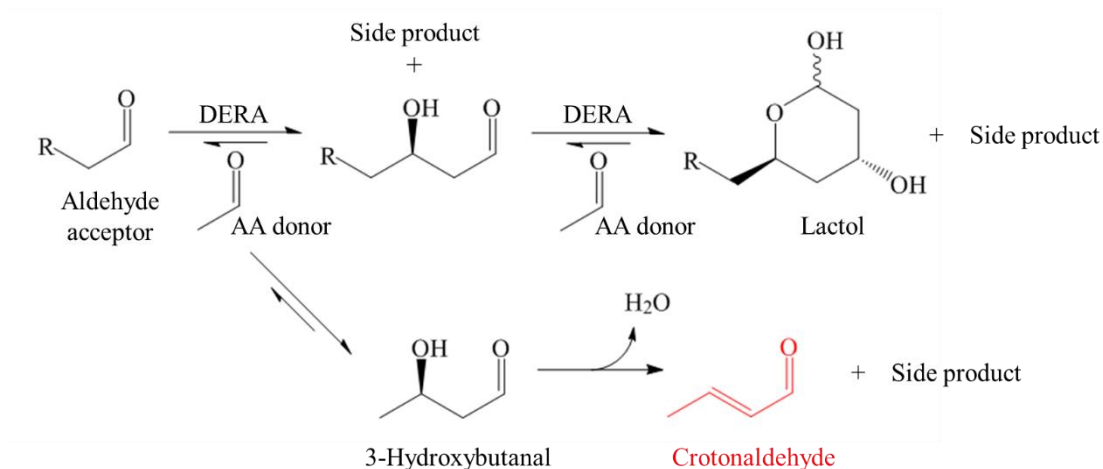
Figure 2.9: DERA-catalyzed reaction forming a key statin side chain intermediate lactol and associated side products. The side product responsible for mechanism-based DERA inhibition is indicated in red [48], [52].

The C47 residue does not have catalytic activity and Dick et al. has developed an acetaldehyde resistant *E. coli* DERA mutant (C47M) by substituting C47 with methionine using site-directed mutagenesis [48]. This mutated DERA variant expressed exceptional catalytic properties that were tested with several aldehyde acceptors and acetaldehyde donor [48]. No further implementation of this C47M DERA mutant was reported. The mutated enzyme's potential to catalyze sequential aldol reaction with minimal to no substrate inhibition makes it an excellent candidate for further application in statin side chain synthesis and process development.

An expression plasmid, pET21a_deOC_EC_C47M_6xhis, containing the C47M DERA mutant gene was provided by Jörg Pietruszka, Ph.D., Research Center Jülich, Germany. Plasmid nomenclature description is provided below in Table 2.2. Lyophilized whole cells containing the C47M DERA mutant protein were used in all biocatalytic steps of this thesis.

Table 2.2: Description of the plasmid nomenclature containing the C47M DERA mutant gene.

Plasmid Nomenclature	Description
pET21a	Plasmid for Expression by T7 RNA polymerase
deOC	DERA-coding gene
EC	Escherichia coli
C47M	Mutant designator
	Indicates substitution of cysteine residue at position 47 with methionine residue
6xhis	C-terminal histidine tag (×6) for affinity purification enhancement

2.4 Manufacturing Processes

2.4.1 General Overview

A manufacturing process is comprised of sequential unit operations, such as filtration or crystallization, which convert raw materials into useful products. In general, either individual unit operations or the whole manufacturing process can be classified into four modes: batch, continuous, fed-batch (semi-batch), and semi-continuous processes [13], [53].

In batch manufacturing, or batch process, all materials are charged before the process start and discharged after the process end. In continuous manufacturing, material is simultaneously charged and discharged during the process. Industrial scale continuous processes operate 24 hours a day and 7 days a week with planned shutdown for maintenance only. In the fed-batch process, material is added, or fed, to the batch reactor but discharged at the end of the process. Semi-continuous manufacturing mimics its continuous counterpart but for a discrete period of time [13], [53]. A schematic representation of these manufacturing processes is demonstrated in Figure 2.10.
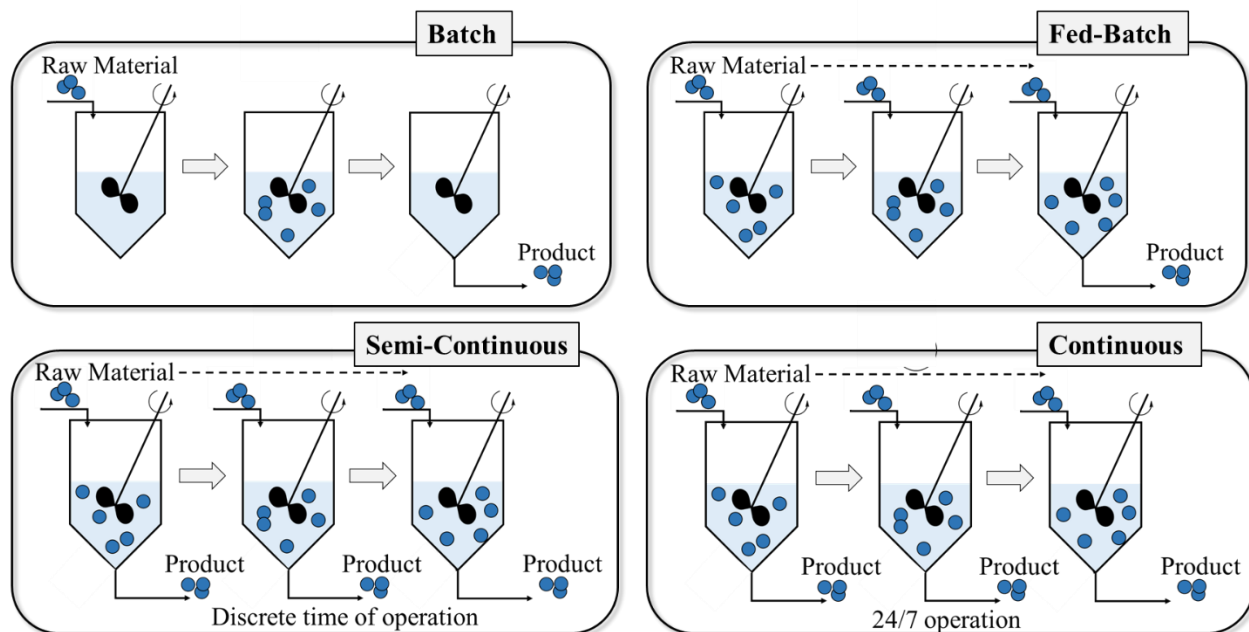
Figure 2.10: General schematic representation of the batch process (top left), fed-batch process (top right), semi-continuous process (bottom left), and continuous process (bottom right) [53].

Continuous processes have been widely implemented on industrial scale by oil refinery, paper, and food industries [13], [14], [54]. The pharmaceutical industry, on the other hand, predominantly manufactures products using batch processes [12], [54]. It is a well-established method for the production of pharmaceuticals incorporating several simple and multi-purpose unit operations. Several steps of the whole batch manufacturing process might be done in different locations, within the facility's country or outside of its borders. Quality control of the product of each process step is usually tested off-line and sometimes can be outsourced to different organizations [12], [13]. Material transportation between different facilities increases the overall production time and raises the capital cost. If the tested samples of a "batch" – a specified quantity of the product – do not have uniform character and quality, the whole "batch" is discarded. These quality discrepancies also happen between "batches" leading to "batch-to-batch" variations. In other words, batch manufacturing can result in supply chain interruptions, long production time, inconsistent product quality, and inability to rapidly increase production quantity in case of drug shortage [11]–[13].

The batch processing drawbacks have slowly pushed the pharmaceutical manufacturing sector towards development and integration of continuous manufacturing [12], [13], [55]. The transition is also supported by the regulatory authorities [12], [13], [53], [56]. Dr. Janet Woodcock, the director of the Center for Drug Evaluation and Research (CDER) at the Food and Drug

Administration (FDA), commented on the pharmaceutical manufacturing trends at the American Association of Pharmaceutical Scientists (AAPS) Annual Meeting in 2011: "Right now, manufacturing experts from the 1950s would easily recognize the pharmaceutical manufacturing processes of today. It is predicted that manufacturing will change in the next 25 years as current manufacturing practices are abandoned in favor of cleaner, flexible, more efficient continuous manufacturing" [53].

2.4.2 Continuous Process Overview

During continuous processing, also known as flow chemistry and CM (continuous manufacturing), a product of one unit operation is directly fed to the next unit operation, which produces a feed stream of the subsequent process, either in a small or large scale. CM combines segregated unit operations of the batch process into a single system. A schematic flow-diagram of an arbitrary and simplified continuous manufacturing process of tablet production is shown in Figure 2.11.
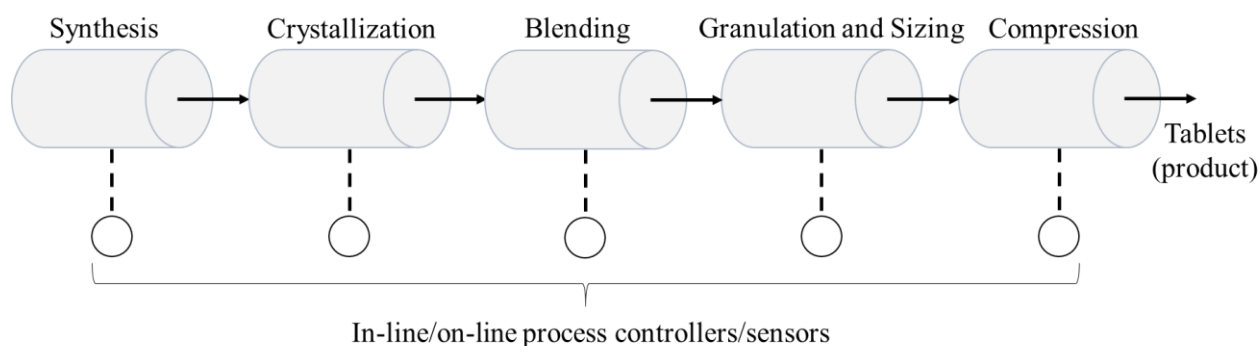
Figure 2.11: Schematic flow-diagram of an arbitrary and simplified continuous manufacturing process of tablet production [12].

CM has many advantages over the conventional batch processing and can provide potential solutions to known batch manufacturing problems [12], [53], [54], [57]. CM integration benefits include reduction of processing time, increase of efficiency, and shortened drug supply chain due to the end-to-end manufacturing, which covers all aspects of the process steps and usually doesn't require services from a third party [12], [13], [53], [58]. The in-line/on-line quality monitoring and control guarantee consistent product quality. Agility of the continuous manufacturing has a straight forward scale-up process and is easily adaptable for the varying demands of production quantity. Multi-step equipment and quality control unit elimination reduce floor space and energy consumption and lower capital costs.

Furthermore, small scale CM is beneficial for the bulk drug substance and API synthesis (primary manufacturing). Reduced equipment size increases surface-to-volume ratio and decreases safety concerns associated with unstable intermediates, high pressure and temperature, and hazardous material utilization and generation [12], [13], [54], [55]. These benefits lead to the increased sustainability of the overall manufacturing processes and to a significant decrease of the environmental foot print of the pharmaceutical industry [54]–[56], [58].

There are some drawbacks of CM that have prevented pharmaceutical companies from implementing continuous manufacturing processes [12], [56]. Major financial investment required for the transition is one of the main reasons companies keep manufacturing running in batch. Additionally, insufficient CM process knowledge requires further process investigation internally. CM process and quality control requires development and integration of higher level process design; however, there is a deficiency in qualified personnel for CM implementation and development. An incomplete set of regulatory documents for CM adds an additional concern for the pharmaceutical companies.

However, considerable investment of effort and finances into the CM move the CM progress forward. To date, the FDA has approved five products produced by continuous manufacturing in the last five years [59]. A list of the approved CM products, product indication, FDA approval date, and company is provided in Table 2.3. Approximately 20 more companies are developing and implementing continuous manufacturing into their production lines [59]. The growing interest and progress in CM have encouraged the FDA to draft a guidance document "Quality Considerations for Continuous Manufacturing" in February, 2019 [60].

Table 2.3: List of FDA approved products manufactured using CM. The list includes product indication, company, and FDA approval date**.** (*) indicates EMA approved product [59], [61].

No.	Product Name	Indication	Company	Approval Date
1	Orkambi (lumacaftor / ivacaftor)	cystic fibrosis	Vertex Pharmaceuticals	July 2015
2	Prezista* (darunavir)	HIV-1 infection	Janssen Pharmaceuticals	July 2016
3	Verzenio (abemaciclib)	breast cancer	Eli Lilly and Company	February 2018

No.	Product Name	Indication	Company	Approval Date
4	Symdeko (tezacaftor/ivacaftor and ivacaftor)	cystic fibrosis	Vertex Pharmaceuticals	February 2018
5	Daurismo (glasdegib)	acute myeloid leukemia	Pfizer	November 2018

Furthermore, different process development approaches are applied for CM and batch manufacturing. Continuous processes are dynamic and require process flow characterization. Residence time distribution (RTD) provides information about the time material spends in the reactor and is further used for adequate process development. Therefore, it is critical to determine the RTD for the processes operated in flow [13].

2.4.3 Residence Time Distribution

The residence time is defined as the total amount of time a fluid element spends inside the reactor. It is a function of reactor volume and velocity of the fluid element. The distribution of time that various fluid elements spend inside the reactor is called the residence time distribution (RTD). Velocity fluctuations inside the reactor produce back mixing, which affects the velocity of each single fluid element. The resultant residence times deviate from the predicted times and affect the overall RTD, hence, affecting the reaction time. In order to correctly predict fluid behavior in the reactor, the RTD is determined experimentally with a tracer. A tracer is an inert chemical, usually a dye, which is fed into the reactor for a certain period of time. The outlet concentration of a tracer is measured and used for RTD calculations. One way to obtain the outlet concentration is to use dye as a tracer and to measure the absorption signal using UV-vis.

The two most common tracer injection methods for the RTD experiments are pulse and step inputs [62], [63]. During the pulse input, a tracer is suddenly injected into the reactor for a very short period of time. It causes a rapid change of the input signal's amplitude. During the step input, a tracer is injected into the reactor at time $t = 0$ until the signal at the reactor outlet reaches a constant value (100 % tracer). Both input strategies are represented as a function of input and output signals and time in Figure 2.12. The detected output signal corresponds to the tracer concentration and is used for RTD calculations. Step input was used to determine the RTD of the reactants flowing through reactor column in this master's thesis.
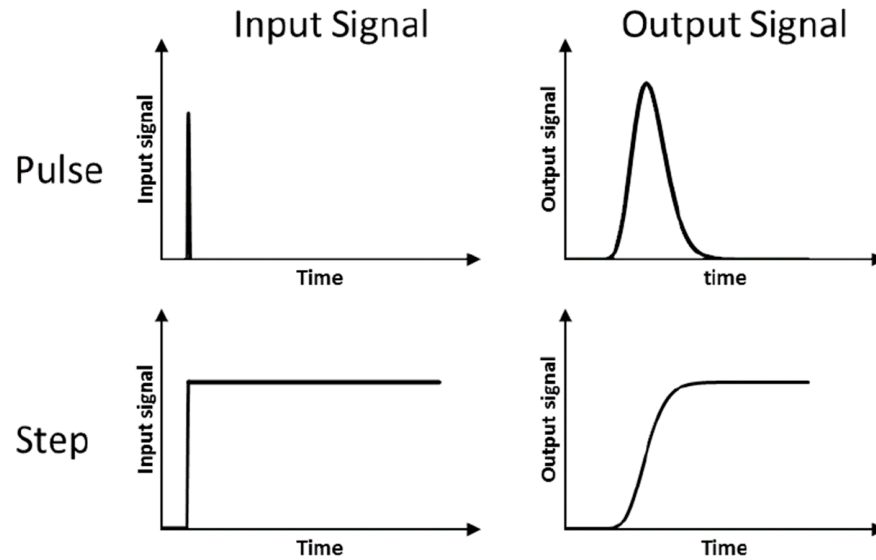
Figure 2.12: Pulse and step input and output signals as a function of time in non-ideal reactors [63].

RTD theory assumes a steady-state system, incompressible flow, and fluid transport by advection [13]. The residence time distribution function $(E(t))$, also known as the exit age distribution, is defined as:

$$E(t) = \frac{c(t)}{\int_0^\infty c(t)dt} \tag{2.1}$$

where $c(t)$ is the concentration of a tracer measured at the outlet of the reactor. The normalized concentration vs. time profile gives the cumulative distribution function $(F(t))$. $F(t)$ represents a fraction of fluid elements that spend a certain amount of time t or less in the reactor. Experimentally determined $F(t)$ is based on the relative output signal of the tracer over time. The relative output signal is defined as the ratio of the signal to the maximum signal obtained. The relationship between the residence time distribution and the cumulative distribution is described as:

$$E(t) = \frac{dF(t)}{dt} \tag{2.2}$$

The mean residence time $\bar{t}$ is defined as:

$$\bar{t} = \int_0^\infty t \cdot E(t)dt \qquad (2.3)$$

The spread of the residence time distribution function is measured by the variance σ^2 and is defined as:

$$\sigma^2 = \int_0^\infty (t - \bar{t})^2 \cdot E(t)dt \qquad (2.4)$$

The dispersion model was used for flow representation in this master's thesis. The dispersion model uses a dimensionless number to characterize longitudinal spread of the flowing tracer in the reactor affected by all acting factors [62]. The dimensionless number is the dispersion number, D/uL, where D is the longitudinal dispersion coefficient, u is the superficial velocity of the flow, and L is the reactor length. Open-open vessel boundary conditions were applied for calculating the dispersion number. Open-open vessel boundary conditions assume an undisturbed flow of the tracer through the boundary conditions and is represented in Figure 2.13 [62], [63].
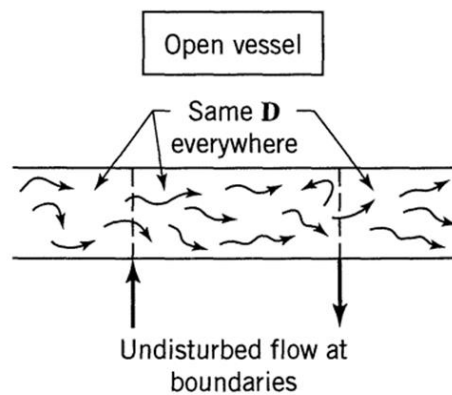
Figure 2.13: Open-open boundary conditions to the reactor [63].

The dispersion number for the open-open conditions is defined as:

$$D/uL = \frac{1}{8}\left(\sqrt{8\bar{\sigma}^2 + 1} - 1\right) \tag{2.5}$$

where $\bar{\sigma}^2$ is $\sigma^2/\bar{t}^2$.

If the RTD experiments yield small D/uL values ($D/uL < 0.01$) then there are small deviations from the ideal plug flow (low back mixing). If the RTD experiments yield D/uL values greater than 0.01 ($D/uL > 0.01$), then the flow behavior deviates from plug flow (high back mixing) [62], [63].

2.5 Enzyme Immobilization

2.5.1 General Overview

Enzyme immobilization is the process of confining an enzyme or cells to an insoluble support material or matrix that is in a different phase than the substrates and products [36], [37]. This confinement creates a heterogeneous system, separating the enzyme from a reaction mixture and limiting its mobility. The enzyme is retained on the support and can be reused several times, and the purification process of the enzyme-free product stream is significantly simplified [14], [36], [37], [64]. Enzyme immobilization may also enhance biocatalytic properties by increasing enzyme's stability [14], [36], [37], [64]. However, immobilization may also limit mass transfer during the process, decreasing the overall yield [64]. In order to limit the effects of poor mass transfer, the immobilization procedure must be carefully optimized by screening several immobilization techniques and conditions while observing the enzyme's behavior [15], [64].

A wide variety of immobilization techniques exist and are applied in industrial settings. These techniques can be divided into several different categories. The most common immobilization categories are entrapment, cross-linking, and carrier bound (solid support) [15], [36], [64]. A simplified schematic representation of these immobilization technique categories is shown in Figure 2.14.
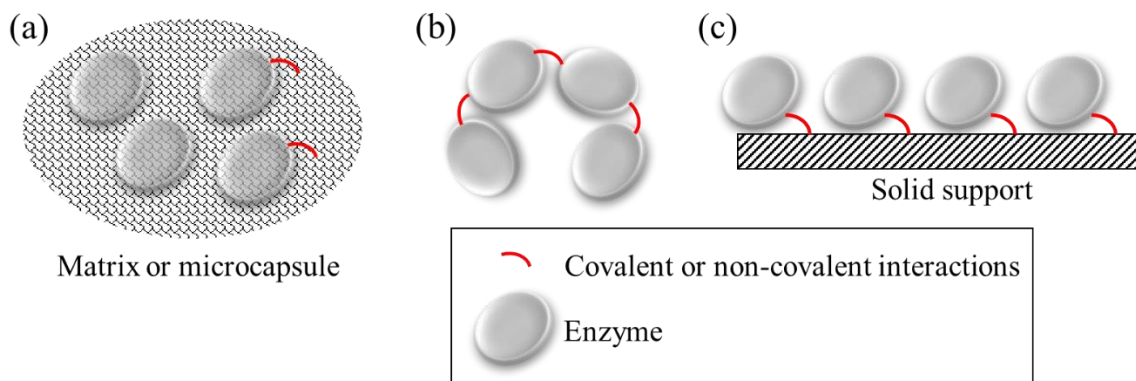
Figure 2.14: Simplified schematic representation of the immobilization categories: (a) enzyme entrapment inside a cross-linked polymer matrix (interaction with the matrix is shown in red) or microencapsulation (no interaction); (b) cross-linking of enzymes; (c) enzyme immobilization on a solid support [15].

The entrapment technique immobilizes an enzyme by trapping it inside a matrix, such as a cross-linked polymer, or by enclosing it inside a semi-permeable microcapsule [14], [36], [64]. This is a relatively simple immobilization method that does not include chemical modification, has no impact on enzyme's intrinsic properties, and decreases the required enzyme quantity [64]. The main disadvantages of enzyme entrapment are enzyme leaching and diffusional constraints that have an impact on enzyme activity [64]. Cross-linking immobilization technique involves a cross linking agent, such as glutaraldehyde, that forms an amide link with either the enzyme, enzyme crystals or precipitated enzyme aggregates [15], [37], [64]. Depending on the state of the enzyme, the cross-linking immobilization drawbacks span from lowered enzyme physical stability, complications associated with crystallization, and enzyme conformational stability [15], [64]. Carrier bound enzymes are immobilized on a solid support by either covalent bonding or non-covalent bonding, such as adsorption or affinity ligands [14], [15], [64]. The solid support plays a crucial role on the immobilization performance and thus must meet strict criteria that include large surface area, mechanical strength, water insolubility, and chemical and thermal stability [14], [15].

In addition to the advantages of enzyme immobilization outlined above, immobilized enzymes are also beneficial in flow experiments [14], [15]. The continuous process is greatly simplified when the flow reactor is packed with immobilized enzyme. However, substantial amount of factors affect enzyme immobilization performance and significant efforts are required for screening and optimizing the immobilization strategies to achieve satisfactory results [15], [64]. Therefore, it is advised to keep the immobilization technique as general as possible to simplify the optimization process [15].

2.5.2 DERA Immobilization for Applications in Continuous Flow

The immobilization technique used in this project involved entrapping DERA in a sodium alginate gel matrix and further immobilizing the enzyme matrix on a loofa sponge by cross-linking the gel with calcium ions onto the solid support. This immobilization strategy was named the alginate-loofa matrix (ALM) by Phisalaphong et al. [65]. Alginate is a naturally occurring anionic polymer that is biodegradable, has low toxicity and cost, and follows a simple procedure to manipulate the degree of polymerization, and hence the strength of the polymer [66], [67]. Loofa sponge (*Luffa cylindrica*) is a readily available biodegradable natural material with low density and high porosity that promotes the mass transfer [65], [68], [69]. Therefore, ALM is an environmentally friendly, cost efficient, prospective, and simple immobilization strategy.

Loofa sponge is derived from fruit of *Luffa cylindrica* plant [69]. It is cylindrical in shape and composed of interconnecting fibers, as illustrated in Figure 2.15. It has good mechanical properties and can withstand harsh process conditions, such as pH extremes and high temperatures [68], [69]. Furthermore, loofa sponge can be recycled after being washed and autoclaved [68]. These parameters make loofa sponge a strong solid support candidate for cell immobilization.

Figure 2.15: Loofa sponge and the enlarged core showing interconnecting fibers.

Alginate is a block copolymer that consists of L-guluronate (G) and D-mannuronate (M) residues [66]. These residues appear either consecutively or alternating in a block and their content varies depending on the alginate seaweed source [66]. The alginate gel is formed by cross-linking the G-blocks of sodium alginate salt with divalent cations, such as calcium, Ca^{2+} [66], [67]. It is believed that M-blocks do not participate in ionic cross-linking [66]. General structures of alginate M and G blocks, and the ionic cross-linking between the sodium alginate salt and Ca^{2+} are illustrated in Figure 2.16. Stability of the cross-linked gel depends on the stability of the links between divalent cation and carboxylate groups [66], [67]. Stability can be manipulated by the type of divalent cation used, and the duration and temperature of the cross-linking process [66], [70].
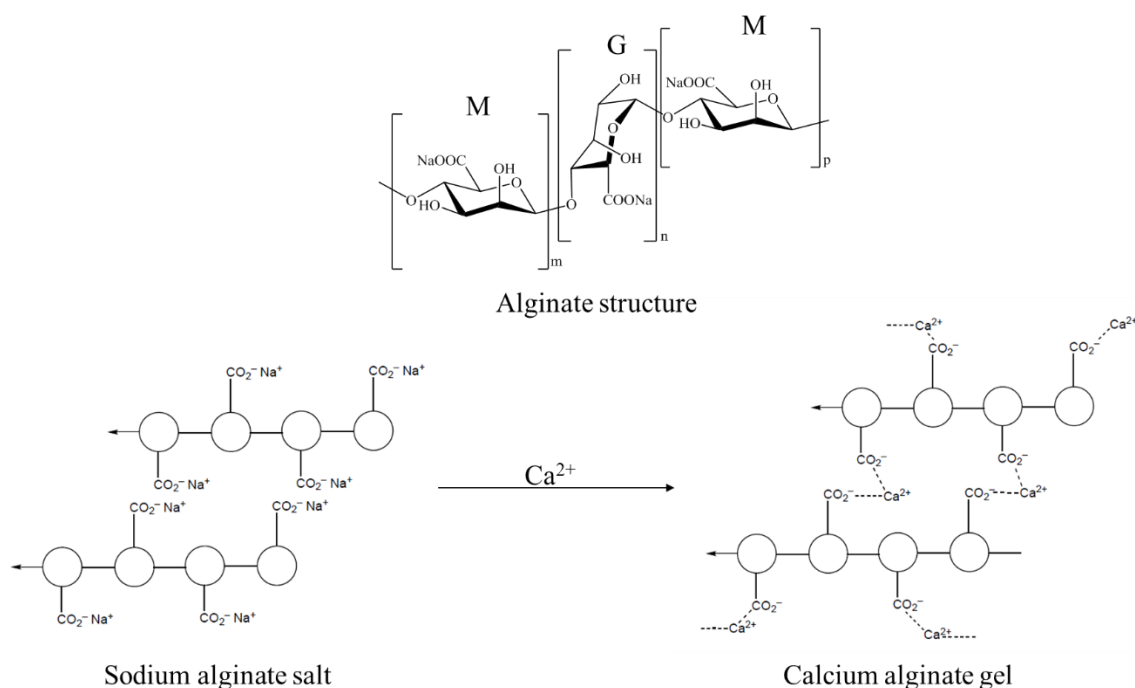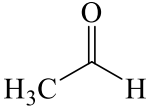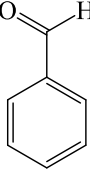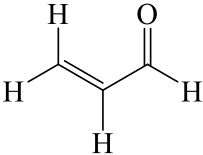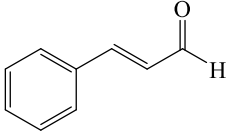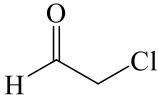
Figure 2.16: L-guluronate (G_n) and D mannuronate (M_m and M_p) blocks of alginate (top) [67]; Ionic cross-linking process from sodium alginate salt (bottom left) to calcium alginate gel (bottom right) [71].

3 Results and Discussion

3.1 Substrate Screening

Five aldehyde substrates were screened in batch for further application in an in-flow DERA-catalyzed step of statin side chain synthesis. The substrates and their molecular structure are listed in Table 3.1. These substrates were tested for their feasibility to act as acceptors for the DERA-catalyzed aldol addition reaction in continuous flow. Acetaldehyde (AA) is a natural donor substrate of DERA and thus AA was a donor in all reactions described in this thesis [34], [40], [41]. Experimental set-up of the batch reactions is described in Section 5.3.

Table 3.1: Aldehyde substrates used for DERA catalyzed aldol reaction and screened in batch for further applications in flow chemistry experiments.

Substrate Name	Substrate Molecular Structure	Substrate Name	Substrate Molecular Structure
Acetaldehyde		Benzaldehyde	
Acrolein		*trans*-Cinnamaldehyde	
Chloroacetaldehyde			

Non-aromatic aldehydes were analyzed with a GC-FID method described in Section 5.4. The reaction progression was analyzed by comparing the peak areas of the respective substrates, intermediates, side products, and products. However, substrate consumption was approximated due to peak overlap with the solvent peak (MeCN) for all non-aromatic aldehydes. For this reason, the calibration data was regarded as ineffective and is not presented herein. Aromatic aldehydes were

analyzed with an HPLC method described in Section 5.4. Calibration data was obtained by the second supervisor Bianca Grabner, M.Sc., in previous experiments (not shown).

DERA-catalyzed sequential aldol addition between acetaldehyde and substituted aldehydes is presented in Figure 3.1. The desired progression of the reaction is indicated in black. Compound **1** is a dimer formed during the first aldol addition reaction and is considered as an intermediate for the whole DERA-catalyzed process. Structure of a trimer, also referred to as a linear product, is compound **2**. Trimer readily undergoes cyclization to form the final product lactol (compound **3**). The side products with the highest likelihood of occurrence, as reported in published literature, are shown in grey [48], [72]. Acetaldehyde can react with itself even in the presence of another acceptor molecule. This is a known side reaction and henceforth referred to as the AA self aldol reaction.
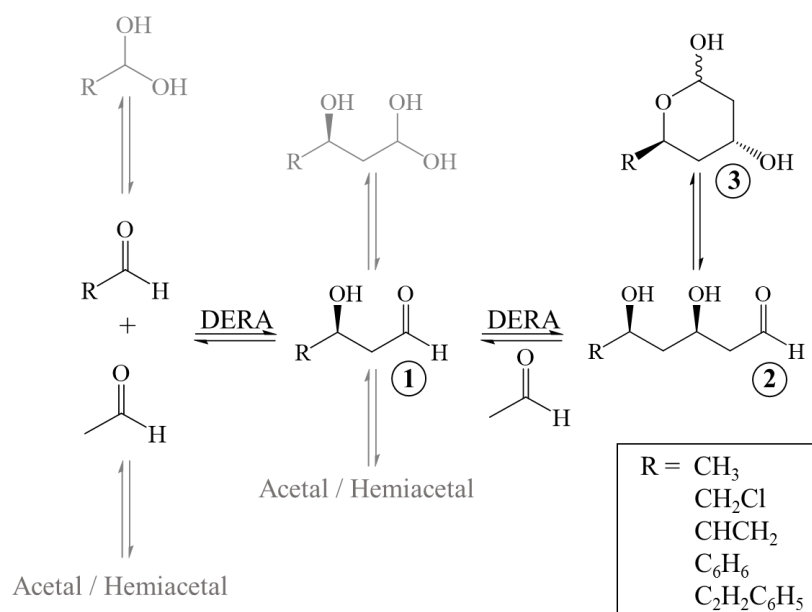
Figure 3.1: The DERA-catalyzed sequential aldol addition between acetaldehyde and substituted aldehydes. Intermediate (dimer) is compound **1**, linear product (trimer) is compound **2**, and product (lactol) is compound **3**. The desired reaction progression is indicated in black. The most possible side products reported in published literature are shown in grey [48], [72].

Five substrates were tested at reaction scales of 0.5 mL, 1 mL, 5 mL, and 50 mL. Reaction scales of 0.5 mL, 1 mL, and 5 mL were tested with 20 mg/mL $DERA_M$ concentration. The largest reaction scale of 50 mL was tested with a concentration of the lyophilized whole cells containing C47M

DERA mutant (DERA$_M$) equal to 2 mg/mL. Same reaction scale using acetaldehyde as both donor and acceptor was tested with 10 mg/mL and 20 mg/mL DERA$_M$ concentrations.

Neither intermediate nor product formation were observed for all five substrates tested with 2 mg/mL DERA$_M$ concentration at 50 mL reaction scale. Reaction of 50 mL with 10 mg/mL of DERA$_M$ produced neither an intermediate nor a product. An intermediate was detected by the GC-FID in the reaction samples with 20 mg/mL of DERA$_M$ after 10 minutes of the 50 mL reaction. No product peaks were detected at any time point analyzed.

The extent of DERA$_M$ expression was assessed by performing sodium dodecyl sulfate-polyacrylamide gel electrophoresis (SDS-PAGE) analysis. The protocol is provided in Section 5.1. DERA$_M$ was detected in all samples analyzed and the results are presented in Figure 7.1. Freeze-dried whole-cell DERA$_M$ pellets were used for the experiments and in whole-cell biocatalysis the cell membrane acts as a mass transport barrier [14], [15], [72]. The lack of the reaction progression was thought to be attributed to mass transport limitations due to cell permeability, insufficient enzyme concentrations, or inactive enzyme.

The results of the 0.5 mL, 1 mL, and 5 mL reaction scales are provided below. Benzaldehyde, cinnamaldehyde, and acrolein were tested with 0.5 mL and 1 mL reaction scales only.

3.1.1 Benzaldehyde and *trans*-Cinnamaldehyde

Reactions with benzaldehyde and cinnamaldehyde as acceptor molecules yielded neither an intermediate nor a product regardless of the reaction scale and DERA$_M$ concentration tested. DERA is capable of accepting a wide number of aldehydes, however, unnatural aldehydes are limited to have a chain of up to four carbon atoms to be well tolerated as acceptors [73]. A lack of DERA-catalyzed aldol reaction progression with cinnamaldehyde acceptor agrees with the results published by Dick et al. who have developed DERA$_M$ and tested its activity towards several acceptor aldehydes [48]. According to the current literature published, benzaldehyde was not previously tested with DERA$_M$. Furthermore, phase analysis performed with Crystalline (Technobis) showed an additional phase present in the reaction mixtures of benzaldehyde (a) and cinnamaldehyde (b), as shown in Figure 3.2. The additional phase is composed of spherical beads that were formed by the aromatic aldehyde in the 0.1 M pH 7.5 TEOA and 0.5 M acetaldehyde solution. The presented images are of reaction mixtures without the lyophilized cells containing

DERA$_M$. Reactions with enzyme pellets produced cloudy images. The additional phase implies poor solubility of both compounds in the 0.1 M pH 7.5 TEOA buffer. The conclusion made based on phase analysis images is supported by the published solubility data of both compounds. The solubility of benzaldehyde in water at 25 °C is 6.95 mg/mL and the reaction requires 53.06 mg/mL (0.5 M) [74]. The soluble concentration of cinnamaldehyde in water at 25 °C (1.42 mg/mL) is exceeded in the DERA-catalyzed reaction (66.08 mg/mL or 0.5 M) [75].
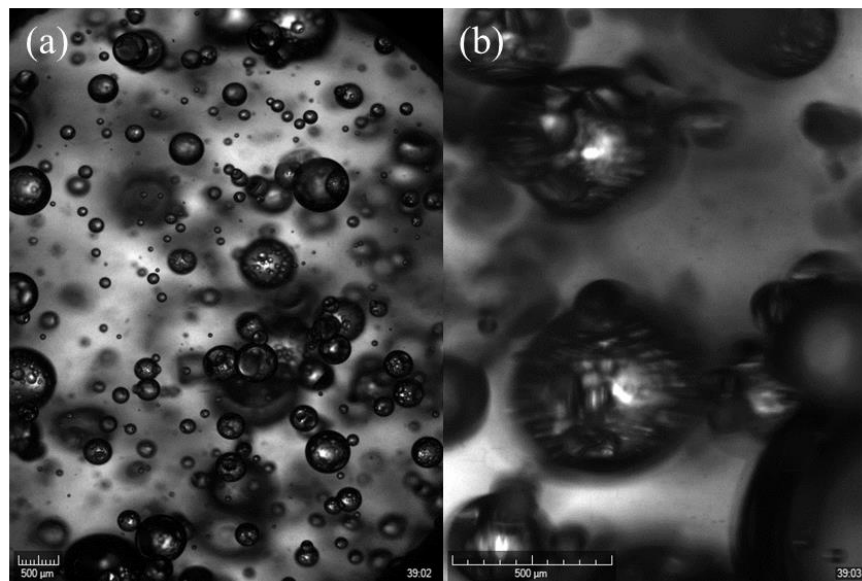
Figure 3.2: Images of spherical beads formed by (a) benzaldehyde and (b) cinnamaldehyde in the reaction mixture of 0.1 M pH 7.5 TEOA and 0.5 M acetaldehyde without lyophilized cells containing DERA under stirring. Pictures obtained using the Crystalline® by Technobis.

Poor solubility of the tested aromatic acceptor molecules limits their accessibility to the active site of DERA$_M$. Therefore, benzaldehyde and cinnamaldehyde were deemed to be poor acceptors for the DERA-catalyzed aldol addition reaction and were not considered for the in-flow DERA-catalyzed aldol reaction experiments.

3.1.2 Acrolein

Acrolein is an α,β-unsaturated carbonyl compound and has a molecular structure similar to crotonaldehyde, a condensation product of the AA self aldol reaction proposed to be responsible for the deactivation of DERA [48]. Molecular structures of both compounds are shown in Figure 3.3. Dick et al. has tested DERA$_M$ activity using acetaldehyde as donor and crotonaldehyde as acceptor. Qualitative HPLC-MS analysis of these experiments demonstrated positive results, but reactions yields were not shown [48].

Crotonaldehyde   Acrolein

Figure 3.3: Molecular structures of crotonaldehyde and acrolein.

Both reaction scales tested yielded neither an intermediate nor a product of the DERA-catalyzed sequential aldol addition between acrolein acceptor and acetaldehyde donor. For the 1 mL reaction volume, GC-FID analysis revealed peaks of the AA self aldol intermediate, the most abundant side product (Figure 3.1) [52]. The respective peak areas were 110.68 a.u. (30 minutes), 348.30 a.u. (60 minutes), and 563.06 a.u. (90 minutes). Several unidentified peaks of side-reactions or impurities were detected for both reaction scales tested.

It was hypothesized that the form of the enzyme used to catalyze aldol addition reactions might be responsible for the slow reaction progression detected by the GC-FID. Dick et al. used purified $DERA_M$ of $\geq 95\%$ purity [48]. The experiments described in the present thesis were conducted with the lyophilized whole cells containing $DERA_M$ with unknown purity. The toxicity of the short chain (C3-C9) aldehydes to the cell as well as interference with other enzymes within the cell could significantly influence the results [76].

Presence of other enzymes in the cell containing $DERA_M$ was verified by the SDS-PAGE results (Figure 7.1). These proteins are not identified and demonstrate one of the main disadvantage of the whole-cell biocatalysis – unknown side reactions [14]. Acrolein and crotonaldehyde are "reactive" aldehydes that can form Michael adducts with thiol and amino groups of proteins [76]. Crotonaldehyde released by DERA as a side product together with acrolein might covalently bind to other cytoplasmic proteins affecting cellular functions and could cause the cytoplasmic concentration of "reactive" aldehydes to reach critical levels. In response, the cell initiates its defense mechanism that triggers release of several enzymes to neutralize these toxic species [77]. The unsaturated short chain aldehydes are oxidized by the protective enzymes thereby creating additional side products and possible completely consuming these aldehydes [77]. It is unknown which cellular functions are affected by the inflated concentrations of acrolein and crotonaldehyde in the cytoplasm. These effects might tamper with the activity of DERA and, as a consequence, with product formation. However, further research is required to understand the exact mechanism behind these processes, which is beyond the scope of the present thesis.

Another factor that could influence reaction progress of the aldol addition between acrolein and AA catalyzed by C47M DERA mutant is another deactivation mechanism [78]. Bramski et al. have tested several DERA variants mutated at C47 position by substituting cysteine with other amino acids [78]. The published data suggests that another acetaldehyde/crotonaldehyde-induced deactivation mechanism may exist independent of C47 residue. The deactivation mechanism has not being identified.

Acetaldehyde and crotonaldehyde may still be hindering DERA activity via an unknown mechanism. Toxic nature of acrolein and crotonaldehyde may contribute to DERA deactivation in addition to tampering with cellular functions and to being oxidized for cell protection. Due to these uncontrolled variables, complex nature of the reaction, and slow reaction progression, acrolein is considered as a non-feasible substrate for the in-flow DERA-catalyzed aldol addition for statin side chain synthesis.

3.1.3 Acetaldehyde

The DERA-catalyzed aldol reaction using AA as acceptor formed an intermediate and a trimer at both reaction scales tested. The peak areas are listed in Table 3.2. No cyclic product peaks were observed.

Table 3.2: GC-FID peak areas of the intermediate and trimer formed by the DERA-catalyzed aldol addition using AA as acceptor for the 0.5 mL and 1 mL scales.

Reaction Volume	0.5 mL		1 mL	
Sample Time [min]	Intermediate	Trimer	Intermediate	Trimer
0			0	0
30	993.29	297.42	4,160.71	845.80
60	1,229.79	485.71	4,855.46	1,293.72
90			5,049.27	1,325.33

The lack of the desired AA product formation might be due to several factors. First, the small-scale reactions were chosen as a preliminary assessment for the DERA$_M$ tolerability of substrates. Therefore, the reaction time may be too short to observe spontaneous cyclization of AA trimer to form the lactol. Second, the rate constant for the intermediate formation is much higher than the rate constant for the trimer/product formation [52]. Ručigaj and Krajnc have presented a kinetic model of a crude DERA lysate-catalyzed sequential aldol reaction using acetaldehyde as donor and

two different acceptor aldehydes, chloroacetaldehyde and acetyloxyacetaldehyde. In the derived model, the formation of the intermediate was 4.2 and 5.8 times faster than the formation of the product for reactions with chloroacetaldehyde and acetyloxyacetldehyde, respectively. The rate of spontaneous cyclization of trimer to the desired product is included in the rate of intermediate to product conversion. Higher rates of intermediate formation was also qualitatively observed by other authors using different enzyme variants [49], [72]. Thirdly, formation of side products due to alternative DERA-catalyzed aldol reactions and other proteins of the cell [14], [72]. Lastly, enzyme deactivation due to a C47-independent mechanism may affect the formation of the desired product and cannot be disregarded despite the unknown mechanism and limited information available [78].

To further analyze tolerability of $DERA_M$ towards acetaldehyde, a 5 mL reaction scale was tested with the identical reaction conditions and formulation: 1.5 M AA (1.0 M donor and 0.5 M acceptor) and 20 mg/mL of freeze-dried *E.coli* cells harboring $DERA_M$ enzyme. The results as GC-FID peak areas are presented in Figure 3.4 below.
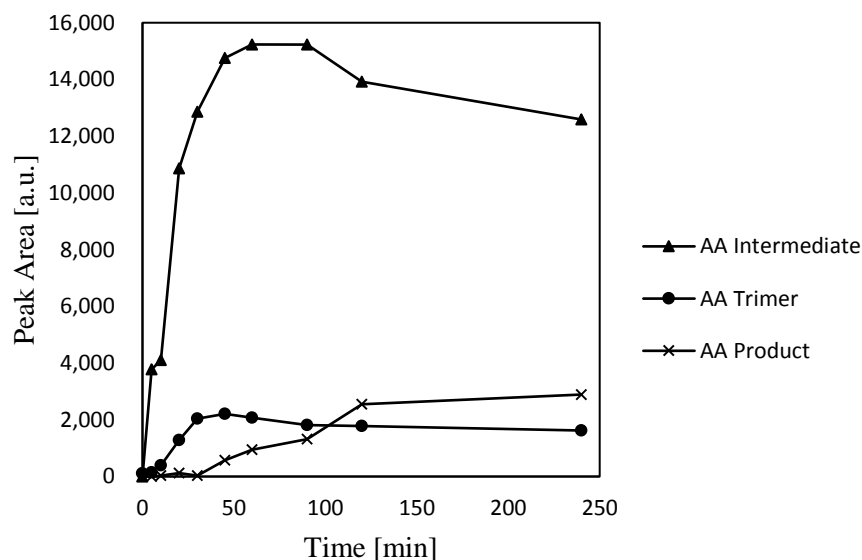
Figure 3.4: GC-FID peak areas of the AA intermediate, AA trimer, and AA product (lactol) formed during a 5 mL DERA-catalyzed aldol addition using AA as acceptor.

Acetaldehyde intermediate is formed much more rapidly than it is consumed for the first 60 minutes of the reaction due to faster intermediate formation kinetics compared to the product formation kinetics [52]. These results agree with the results obtained from the 0.5 mL and 1 mL reactions. The concentration of the intermediate begins to decrease after 90 minutes of the reaction. The acetaldehyde peak was not visible in the GC-FID at the same time point indicating complete

substrate conversion into intermediate, trimer, minor side products, and product. Trimer peak area appears saturated, which allows for more product generation with time. Trimer peak area decreases more slowly in comparison to the intermediate decrease and product area increase. The reaction requires three intermediate molecules to generate one trimer/product when the substrates are completely consumed. Additionally, a decreasing rate of trimer conversion may indicate loss of enzyme activity. Therefore, the available intermediate may be consumed for other competing side reactions.

In Figure 3.4, the equilibrium shift between AA trimer and the cyclic product is most evident after 45 minutes of the reaction after a substantial amount of trimer is already formed with a peak area of 2,208.96 a.u. The corresponding peak area of the product is equal to 125.61 a.u. As stated above, the corresponding peak areas are provided for comparison to further experiments. However, a significant increase in product formation is noticed after the trimer's peak area exceeded 2,000 a.u. The 1 mL reaction produced a trimer peak area of 1,325.33 a.u. at 90 minutes and no product (Table 3.2). No product was formed for the 0.5 mL reaction with the intermediate's peak area of only 485.71 a.u after 60 minutes (Table 3.2). Therefore, it was hypothesized that the cyclization depends on the amount of trimer present in the reaction and high concentration of trimer shifts the equilibrium towards its cyclic form.

Acetaldehyde has proven to be a good potential substrate for the DERA-catalyzed aldol addition reaction in continuous settings due to the evident reaction progression for all reaction scales tested (0.5 mL, 1 mL, 5 mL, 50 mL) with 20 mg/mL enzyme concentration. The reaction progression was determined by the intermediate formation and approximated substrate consumption. Furthermore, the formation of the trimer was detected in reactions of 0.5 mL and 1 mL volume and the desired cyclic product was formed with a 5 mL reaction scale.

3.1.4 Chloroacetaldehyde

Chloroacetaldehyde (CAA) substrate utilized as acceptor in the DERA-catalyzed aldol reaction performed in 0.5 mL and 1 mL scales yielded an intermediate formation only. The peak areas are listed in Table 3.3.

Table 3.3: GC-FID peak areas of the intermediate formed by the DERA-catalyzed aldol addition using CAA as acceptor for the 0.5 mL and 1 mL scales.

	GC-FID Peak Area (a.u.)	
Sample Time [min]	Intermediate – 0.5 mL	Intermediate – 1 mL
0		0
30	887.51	156.63
60	2,366.90	277.05
90		379.10

DERA-catalyzed sequential aldol addition reaction using CAA as acceptor performed better at the 0.5 mL scale than at the 1 mL scale, producing CAA intermediate with an area peak of 2,366.90 a.u. after 60 minutes of the reaction. The reaction of 1 mL volume produced CAA intermediate with a peak area of 379.10 a.u. detected at the end of the 90 minute reaction time. AA intermediate was produced in small quantity for the 0.5 mL reaction volume with an area peak of 43.87 a.u. measured at 60 minutes (data not shown).

Chloroacetaldehyde is a potent electrophile and therefore DERA$_M$ prefers CAA as an acceptor aldehyde over AA. The CAA rate constant was determined to be 6,374 times larger than the AA rate constant by the kinetic modeling of Ručigaj and Krajnc [52]. However, the enzyme variant used for the kinetic modeling is different than the variant used for the experiments demonstrated in this work. It was assumed that the extent of DERA$_M$ acceptor preference is not as drastic compared to the variant used in kinetic modeling due to the DERA$_M$'s modifications associated with AA resistance.

DERA-catalyzed aldol reaction using chloroacetaldehyde as acceptor demonstrated no trimer or product formation for the 2 reaction scales tested. Kinetic modeling derived by Ručigaj and Krajnc for the DERA-catalyzed reaction using chloroacetaldehyde as acceptor determined an inactivation constant for CAA as 9.4 times larger than an inactivation constant of AA [52]. DERA$_{WT}$ is known to poorly tolerate non-physiological acceptors, including chloroacetaldehyde, which irreversibly inactivates DERA$_{WT}$ at concentrations above 200 mM [51]. The reactions of 0.5 mL and 1 mL used 500 mM CAA. The modifications of DERA$_M$ triggered acetaldehyde induced inhibition only and the mutant enzyme was not tested using CAA as acceptor [48]. Therefore, in addition to the intermediate consumption by secondary reactions, low reaction yields might be attributed to the enzyme inhibition induced by CAA and AA.

Several publications have demonstrated direct interaction between the serine 238 (S238) residue in the DERA$_{WT}$ active site and the phosphate group of the physiological substrate [44], [45], [47], [51]. Mutation of this residue exhibited higher tolerance of DERA towards non-phosphorylated substrates, including chloroacetaldehyde [51]. Active site residues are not the only residues that participate in substrate binding and conversion. The C-terminal tail of DERA was hypothesized to be just as important for efficient catalysis, however, its exact role is unknown [43], [79]. The C-terminal tail of DERA is an intrinsically disordered region outside of the fold. It was proposed that when tyrosine 259 (Y259) in the C-terminus enters the active site, it participates in catalysis by facilitating the C2 proton abstraction [43]. Additionally, Y259 residue can enter the active site without the substrate present, pre-sampling conformations relevant for enzyme functionality [43]. Another proposed role of the C-terminal tail in catalytic process is substrate tolerance by enhancing active site flexibility [79]. Truncated C-terminal tail of DERA induced conformational changes of residues within the active site thereby increasing substrate specificity towards non-phosphorylated substrates. This implies that the C-terminal tail residue is important for catalytic activity only with physiological substrates and may induce non-physiological substrate tolerance [79]. Several other DERA mutants showed higher tolerance towards non-phosphorylated substrates; however, C49 was not the mutated residue that showed positive results towards higher substrate specificity [43], [47], [51]. Therefore, the C47M DERA mutant is assumed to be inhibited by chloroacetaldehyde just as well as DERA$_{WT}$.

For further investigation of DERA$_M$ tolerance and activity towards chloroacetaldehyde as acceptor, a 5 mL scale was tested with different substrate concentrations. The 5 mL reaction volume was chosen because aldol addition with acetaldehyde as acceptor performed best at that scale. Two molar ratios of the substrates were examined - 1.0 M AA + 0.5 M CAA (2:1) and 0.5 M AA + 0.5 M AA (1:1). Lower molarity of acetaldehyde was tested to evaluate its effect on product formation and enzyme activity. The results are presented in Figure 3.5 (a),(b) below.

Figure 3.5: GC-FID peak areas of the intermediate, trimer, and product formed for the DERA-catalyzed aldol reaction at 5 mL scale using AA donor and CAA acceptor at molar ratios of (a) 2:1 (1.0 M : 0.5 M) and (b) 1:1 (0.5 M : 0.5M). Compounds that belong to primary axis are marked in red.

Aldol addition reaction (a) with 1.0 M acetaldehyde and 0.5 M chloroacetaldehyde (2:1 molar ratio) performed better than the reaction (b) with 0.5 M acetaldehyde and 0.5 M chloroacetaldehyde (1:1 molar ratio). At the end of the 4 hours, reaction (a) yielded an area peak of CAA intermediate and CAA product equal to 6,212.24 a.u. and 2,883.36 a.u., respectively. Higher intermediate formation compared to product formation is caused by the higher intermediate reaction rate [52]. Trimer formation was not detected, most likely because of the large amount of CAA product formed, which shifted the equilibrium towards the cyclic compound. CAA intermediate and CAA

product consumption was detected after 60 minutes of reaction time with peak areas of 7,272.01 a.u. and 3,229.06 a.u., respectively. Additionally, both substrate peaks were visible even in the 4 hours samples. CAA product consumption might be attributed to either retro-aldol reaction or unknown side reactions that consume CAA product. However, the likelihood of the retro-aldol reaction is low because complete, or nearly complete, consumption of one of the substrates is required for its occurrence.

AA trimer formation continued for the whole reaction course after its formation was detected at 120 minutes with an area peak of 10.47 a.u. The peak area of AA trimer at 4 hours was 50.13 a.u. A slow AA trimer formation and AA intermediate consumption evident throughout the 4 hours tested is an indication of a slightly active $DERA_M$. Additionally, enzyme substrate specificity might prefer AA, its natural substrate, with the chloroacetaldehyde-induced deactivation thereby no more CAA-AA cross reaction compounds are formed. However, AA self aldol trimer is formed at a very slow rate in addition to other side reactions. This interesting switch of substrate specificity towards AA during CAA-inactivation may be partially attributed to the modifications that made C47M mutant more resistant to AA inhibition.

Aldol addition reaction (b) with 0.5 M acetaldehyde and 0.5 M chloroacetaldehyde (1:1 molar ratio) favored AA self aldol side reaction more than the reaction (a). At the end of the 4 hours, the area of the AA intermediate and AA trimer peaks were equal to 132.29 a.u. and 71.57 a.u., respectively. Reaction (b) produced less of the CAA product compared to reaction (a) with an area of 529.70 a.u. at 4 hours, which is lower than the CAA peak area detected at 2 hours (561.99 a.u.), indicating a slow consumption of CAA product by the retro-aldol reaction or side reactions. Lower production rates of CAA product compared to reaction (a) are attributed to the CAA-induced inhibition and a limited amount of donor molecules available in the reaction mixture. The concentration of acetaldehyde in reaction (b) is half of the concentration used for reaction (a). Additionally, a portion of the AA molecules is consumed for the side reactions such as AA self aldol reaction, which is evident by AA trimer formation. As with reaction (a), CAA product consumption and AA trimer formation might be attributed to the switch of $DERA_M$ substrate specificity caused by CAA-induced inhibition and the mutations at the C47 residue.

As shown in Figure 3.5, chloroacetaldehyde significantly contributes to enzyme inhibition. It was hypothesized that lower concentration of both substrates at a 2:1 donor : acceptor molar ratio slows

down the substrate-induced enzyme deactivation due to low surplus of the reactants while producing the desired CAA product at a competitive rate due to the optimal donor : acceptor molar ratio [49]. To evaluate this hypothesis, a 5 mL DERA-catalyzed sequential aldol reaction using CAA as acceptor was tested. A reaction time of 30 minutes was chosen for a quick reaction behavior analysis. The results are presented in Figure 3.6.
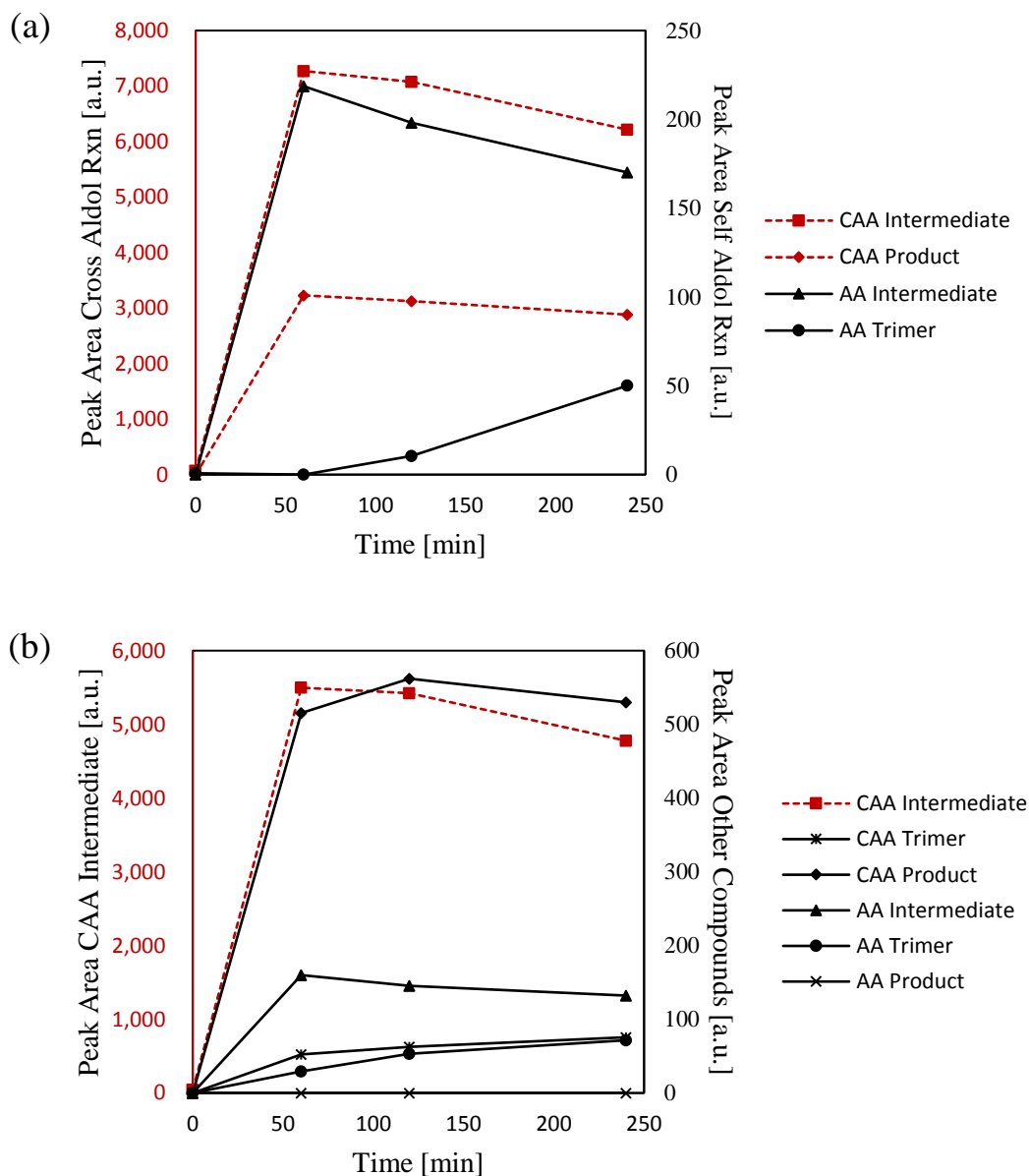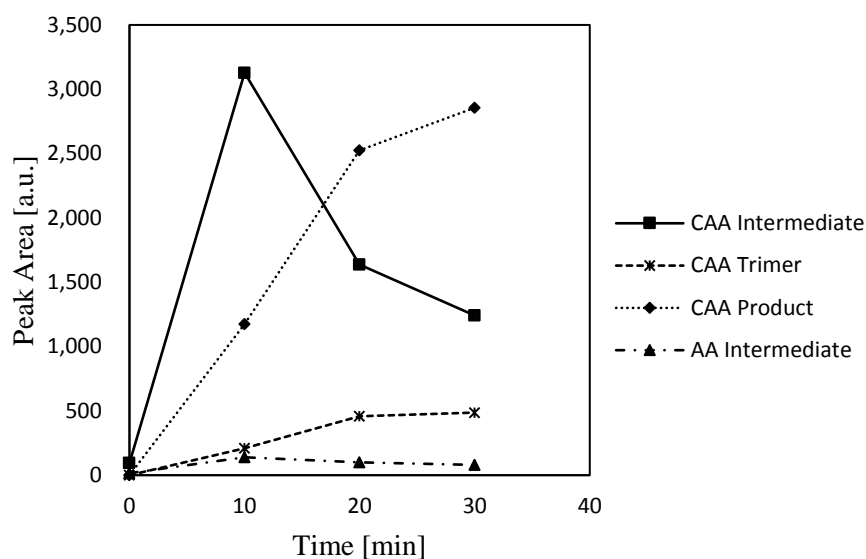

Figure 3.6: GC-FID peak areas of the intermediate, trimer, and product formed for the DERA-catalyzed aldol reaction at 5 mL scale using AA donor and CAA acceptor at molar ratio of 2:1 (0.5 M : 0.25 M).

At the end of the 30 minutes, the peak areas of the CAA intermediate and CAA product were 1,242.16 a.u. and 2,856.24 a.u., respectively. CAA intermediate consumption was already observed after 10 minutes. CAA product consumption is not present in the time period tested, however, the rate of CAA product formation has declined after 20 minutes. This CAA product peak area value at 30 minutes is close to the CAA product peak area of reaction (a) (Figure 3.5) at 60 minutes with a value of 3,229.06 a.u. Additionally, CAA trimer is not fully converted to its cyclic form by the end of the reaction having a peak area of 486.76 a.u. This is the highest area of the CAA trimer peak observed in the 5 mL reactions tested. Even though the tested reaction time for the 0.5 M AA and 0.25 M CAA reaction is shorter than the reactions (a) and (b) (Figure 3.5), it is still important to highlight the rapid rate of the reaction presented in Figure 3.6 despite the halved initial concentration of substrates. Another interesting observation is the lack of AA trimer formation and an apparent consumption of the AA intermediate after 10 minutes. Additionally, AA intermediate peak area at the end of the 30-minute time point is significantly smaller (79.40 a.u.) compared to the AA intermediate peak areas of the reactions (a) and (b) (Figure 3.5) with values of 218.16 a.u

and 159.91 a.u., respectively. The enzyme did not divert towards AA substrate as an acceptor most likely due to the low inactivation rates caused by lower substrate accumulation at the active site [27], [49], [72]. Therefore, competitive CAA product formation rates, lack of CAA product consumption, presence of CAA trimer for further cyclization to the CAA product, and low yields of the AA self aldol side reactions demonstrate a more efficient enzyme and thereby an improved reaction.

3.1.5 Substrate Decision

DERA-catalyzed sequential aldol addition reactions using acetaldehyde (AA reaction) and chloroacetaldehyde (CAA reaction) as acceptors are both good candidates for further applications in continuous synthesis. Enzyme inhibition is evident in both cases, however, CAA is a more potent inhibitor. CAA reaction performed best with 0.5 M AA and 0.25 M CAA. The side reactions are unknown in both instances, but the CAA reaction also experiences the AA self aldol side reaction.

Continuous addition of substrates minimizes enzyme deactivation and side product formation by decreasing substrate accumulation in the reaction mixture. Performing DERA-catalyzed aldol reactions with $DERA_M$ using chloroacetaldehyde as an acceptor in continuous settings is thus hypothesized to minimize chloroacetaldehyde induced inhibition and to improve product yields. Additionally, fed-batch regime is constructed for the aldol reaction catalyzed by $DERA_M$ using CAA as an acceptor to push the reaction towards product formation for further product characterization (Section 3.3.2). The results of batch and fed-batch regimes are compared to the performance of the continuous reactor with immobilized enzyme. The CAA disadvantage of having higher deactivation constant compared to AA makes it an attractive substrate for comparison of the three modes of synthesis with the same enzyme variant [52]. Therefore, chloroacetaldehyde is chosen as a substrate for the in-flow experiments with $DERA_M$ to demonstrate the effects of continuous synthesis on productivity and substrate-induced enzyme inhibition compared to batch and fed-batch reactions performed with the same substrates and enzyme.

3.2 $DERA_M$ Concentration Screening

Three concentrations of $DERA_M$ – 20 mg/mL, 40 mg/mL, and 80 mg/mL – were tested in batch to analyze an increase in enzyme concentration and its effects on the aldol addition reaction

progression for reaction behavior analysis and further comparison with reactions in continuous settings. Experimental set-up of the DERA$_M$ concentration screening in batch is described in Section 5.3. The results are illustrated in Figure 3.7 below.
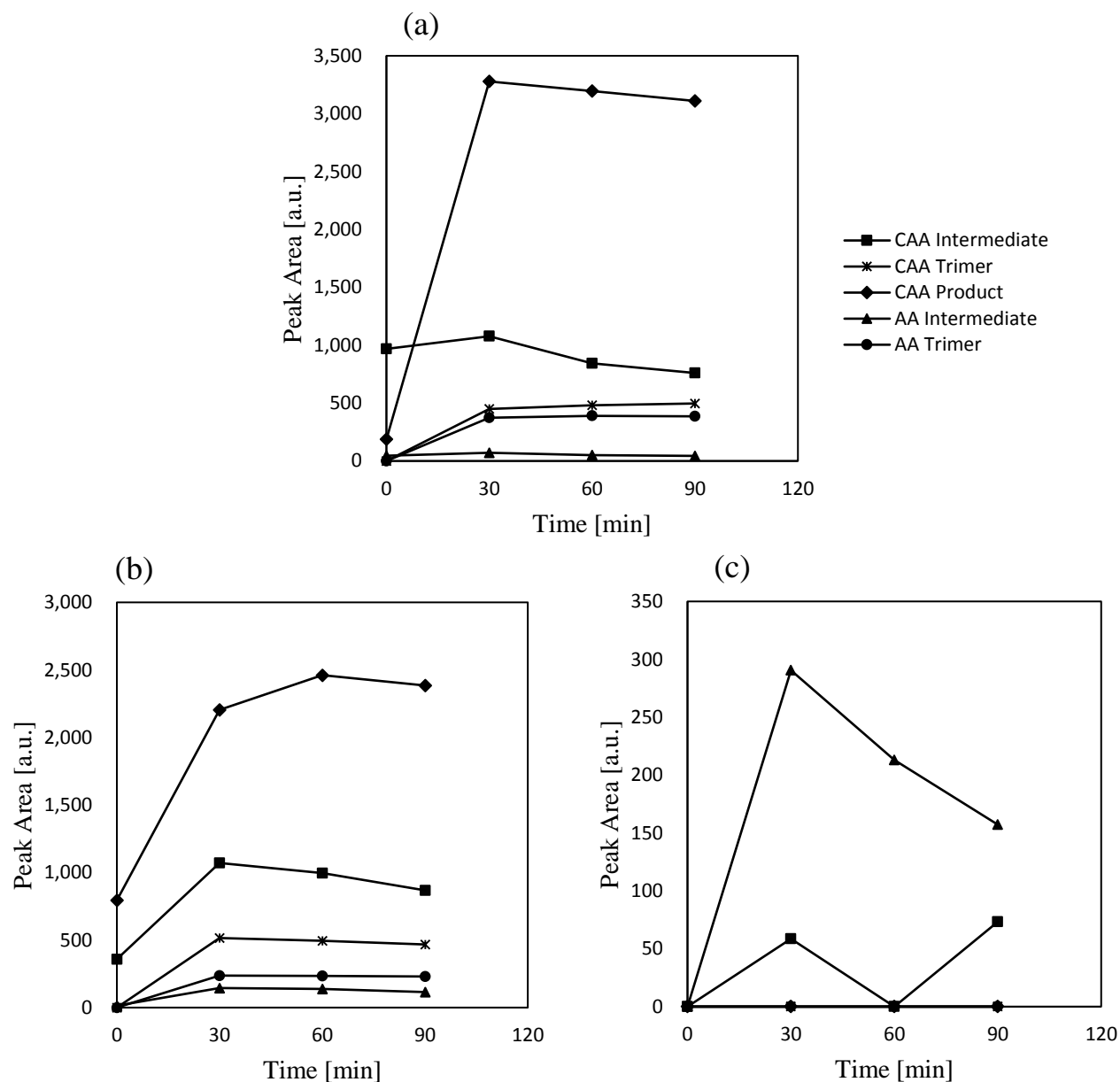
Figure 3.7: GC-FID peak areas of the intermediate, trimer, product, and side product formed for the DERA-catalyzed aldol reaction at 5 mL scale using AA donor and CAA acceptor at molar ratio of 2:1 (0.5 M :0.25 M) with a concentration of the whole-cell containing DERA$_M$ (a) 20 mg/mL (b) 40 mg/mL (c) 80 mg/mL.

The slowest reaction progression was observed with the highest freeze-dried cell concentration of 80 mg/mL (Figure 3.7 (c)), where peak areas of only two compounds were detected – AA self aldol side reaction intermediate and CAA intermediate. The main reason for the poor reaction

performance is the formation of clusters by the lyophilized cell pellets at such high concentrations. Cell clusters formation decreases the surface area available for the reactants to adsorb decreasing the amount of substrates available to form complexes with DERA$_M$. Figure 3.7 (c) represents a case where the enzyme occupied the whole volume of the reaction mixture forming one big cluster and drastically decreasing the amount of sites available for the reactants to adsorb. Additionally, high load of lyophilized whole-cell catalyst decreases mixing efficiency and creates an additional adverse variable during sampling. Each sample taken does not accurately represent the composition of the reaction mixture at the sampled time point due to poor mixing and uneven catalyst and substrates/products distribution throughout the reaction mixture. Therefore, an odd behavior of the CAA intermediate peak area demonstrated in Figure 3.7 (c) is attributed to these factors. However, the peak areas of the AA self aldol intermediate are the highest for the reaction (c) in Figure 3.7 compared to reactions (a) and (b) in Figure 3.7 throughout the whole reaction course. Abundance of biocatalyst available in the reaction mixture might have used up the CAA fairly quickly due to its high electrophilicity and large reaction constants compared to AA [27], [52]. Only a portion of the enzyme present was affected by CAA concentration thus deactivated. Active enzymes thereby formed enzyme-substrate complexes with the only available substrate AA, which in return led to high peak areas of AA self aldol intermediate at high rates. The lack of AA self aldol trimer and product formation is attributed to the increased amount of secondary enzymes present in the reaction with an increased amount of cells added to the reaction. AA gets converted by DERA$_M$ fast, however, competitive side reactions caused by secondary enzymes consume AA and its variants formed with DERA$_M$ aid.

Increase of a catalyst load usually increases the reaction rate of the same volume and substrate molarity. The behavior observed in Figure 3.7 (b) contradicts that statement. Lower reaction yields are caused by the formation of enzyme clusters, poor mixing, and increase in secondary enzymes present. The extent of the reaction impediment depends on the degree of cluster formation, observed in Figure 3.7 (c).

The sequential aldol addition reaction catalyzed by 100 mg of lyophilized whole cells containing DERA$_M$ (20 mg/mL, Figure 3.7 (a)) performed better than reactions catalyzed by 200 mg of cells (40 mg/mL, Figure 3.7 (b)) and 400 mg of cells (80 mg/mL, Figure 3.7 (c)). Reaction (a) and reaction (b) in Figure 3.7 have CAA intermediate and product present at the zeroth time point. CAA is a potent electrophile with a high reaction constant for DERA-catalyzed sequential aldol

addition, therefore it readily gets converted to the intermediate and product. The exact zeroth time point is impossible to analyze because the samples are taken after all components are added to the reaction mixture and the reaction has progressed for a few seconds. Sufficient mixing and easier access of substrates to the cells, and thereby $DERA_M$, allowed the reaction with 20 mg/mL of lyophilized whole cells perform better than reactions with higher concentrations of cells tested.

3.3 Intermediate and Product Characterization

3.3.1 Intermediate Characterization

Experimental set-ups of intermediate synthesis and purification procedure are described in Section 5.5. A monoadduct intermediate of the DERA-catalyzed aldol addition between CAA and AA was synthesized in batch. The most optimal reaction conditions were determined to be with 5 mL reaction volume and 5-minute reaction time. These batch conditions were tested and revealed only the intermediate and no product formation, making them suitable for intermediate characterization by GC-FID analysis following the procedure described in Section 5.4.

Several 5-minute batch reactions were completed with the highest monoadduct yield of 74 mg (48.3 % yield) and the lowest monoadduct yield of 46.2 mg (30.2 % yield) after purification by extraction. GC-FID analysis revealed an intermediate peak of the CAA-AA reaction and unknown side product peaks. As discussed in Section 3.1, both AA and CAA peaks are partially in the solvent peak and their consumption could not be quantified. The final appearance of the intermediate after purification was an amber oily substance, as shown in Figure 3.8.

Figure 3.8: Worked-up monoadduct produced by the DERA-catalyzed sequential aldol addition between chloroacetaldehyde and acetaldehyde (m=46.2 mg; 30.2 % yield).

Due to the reaction scale limitations, low production rates caused by secondary enzymes and $DERA_M$ inhibition, and oily nature of the purified substance the intermediate calibration yielded inconsistent results and was unsuccessful. Therefore, GC-FID peak area comparison is used for the intermediate formation analysis in continuous flow.

3.3.2 Product Characterization

Experimental set-ups of product synthesis and purification procedure are described in Section 5.5. A cyclic product was obtained in a fed-batch regime to avoid enzyme inhibition and push the reaction towards product formation [49]. The purified by extraction product was analyzed with GC-FID following the procedure described in Section 5.4.

Fed-batch process produced 121.3 mg (58 % yield) of the purified substance and the GC-FID analysis displayed AA self aldol side reaction intermediate, CAA intermediate, CAA cyclic product, and unknown side product peaks. As stated above, AA and CAA consumption could not be analyzed due to the observed overlap with the solvent peak. The purified substance from the fed-batch process had similar amber oily appearance as purified intermediate demonstrated in Figure 3.8. Due to the reaction scale limitations, low intermediate conversion and lactol production rates caused by secondary enzymes and $DERA_M$ inhibition, and oily nature of the purified substance the product calibration yielded inconsistent results and was unsuccessful. Therefore, GC-FID peak area comparison is used for the product formation analysis in continuous flow.

3.4 Residence Time Distribution

Residence Time Distribution (RTD) experiments were performed to experimentally determine the mean residence time of the reactants in the column at the given reaction conditions and to determine the dispersion number, D/uL, for a preliminary reactor performance evaluation. The RTD experiments were conducted only for a quick overview of the flow behavior inside the column packed with the loofa sponge and only one RTD experiment was performed per flow velocity. Three flow velocities were analyzed: 0.1 mL/min, 0.25 mL/min, and 0.5 mL/min. The experimental set-up of the RTD experiments is described in Section 5.6. Calculations of the experimentally determined mean residence time, $\bar{t}_{exp}$, $(\bar{t}_{exp} = \bar{t})$ and the experimentally determined dispersion number, D/uL, are described in Section 2.4.3. Calculations for the theoretically determined mean

residence time, $\bar{t}_{th}$, is described in Section 5.6. The results obtained from the RTD experiments were used as a guide in choosing the flow velocity for the continuous statin side chain synthesis experiments. These results are summarized in Table 3.4 below.

Table 3.4: Theoretically and experimentally determined mean residence time and dispersion number for the three test flow velocities going through an HPLC column (20 cm × 0.8 cm) packed with loofa sponge.

v [mL/min]	$\bar{t}_{th}$ [min]	$\bar{t}_{exp}$ [min]	D/uL [--]
0.1	60.5	62.7	0.067
0.25	24.2	26.8	0.105
0.5	12.1	11.4	0.030

The lowest percent difference between the theoretical and experimental mean residence times was observed for the 0.1 mL/min experiment and was determined to be 3.58 %. The highest percent difference of 10.7 % was found for the 0.25 mL/min flow velocity. The experiment ran at 0.5 mL/min yielded a 5.83 % difference between $\bar{t}_{th}$ and $\bar{t}_{exp}$. The observed deviations of the experimentally determined mean residence times from the theoretical values are mainly attributed to the variable active reactor volume available for the reactants to react.

The active reactor volume depends on total sponge volume, sponge void space, and dead zones present inside the reactor. These three factors could not be controlled in the experimental design. The theoretical model, however, assumed constant active reactor volume. For the experiments, the sponges were cut manually in such a way to completely pack the HPLC column without overlapping both cylinders along the length of the column. This helped prevent column blockage. The resultant dimensions of the loofa sponge cylinders slightly varied from one another, as shown in Figure 3.9. Furthermore, a new set of sponge was used at each velocity tested to control the time packed sponges were exposed to the solvent prior to initiating the RTD experiments. This was done to ensure similar mechanical properties of loofa sponge sets in the beginning of each experiment because moisture content influences the mechanical properties of natural sponges [69].
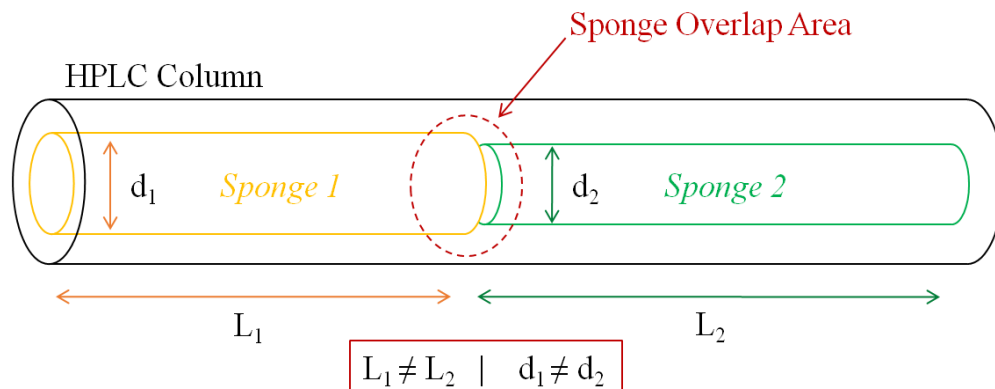
Figure 3.9: Graphical representation of two cylindrically cut loofa sponge pieces packed inside the column, their differences in dimensions, and area of sponge overlap inside the column.

This size inconsistency impacts the sponge volume, V_S, and affects the available active column volume. Sponge void space is an additional factor that could affect V_S. Sponge void space is determined by the interconnecting fibers of the sponge, as illustrated in Figure 2.15. The spatial orientation of these interconnecting fibers is random and varies throughout a single sponge and among sponges.

Another important player in the active reactor volume variability is dead zones. Dead zones are areas inside the reactor where little or no mixing of the reactants occurs. As a consequence, the reaction does not proceed in these regions, leading to a decrease of the active reactor volume. The presence of a dead volume inside the packed column will lead to a shorter mean residence time compared to the theoretically computed values. This time difference was observed for the 0.5 mL/min flow velocity.

The experimental results in the continuous set-up revealed deviations from the ideal plug flow behavior as D/uL values were higher than 0.01. The smallest D/uL value of 0.030 was obtained at 0.5 mL/min and the highest value was found to be 0.105 for the 0.25 mL/min flow velocity. The RTD experiment performed with the slowest flow rate yielded a D/uL value of 0.067. Under the three conditions tested, the system experienced high back mixing, which resembles the behavior of fluid in a continuous stirred tank reactor (CSTR).

Back mixing is observed when reactants and products move at different rates and in different directions along the reactor space. These variations could be caused by the presence of dead zones or channeling of fluid. Channels created inside the column have low flow resistance and allow

some reactants to spend less time inside the reactor [80]. Interconnecting fibers of the sponge and sponges with variable diameter (Figure 3.9) might be responsible for the dead zones and channels. Potential sponge overlap inside the column may create additional dead zones.

The RTD experiments were performed to yield in determining the optimal flow conditions for the DERA-catalyzed aldol reaction in a continuous setting. The varied spatial geometry of the fluid path inside the packed column and inconsistent amount of space available for mass transfer affected the flow pattern causing deviations from plug flow behavior. The factors described above are independent random fluctuations that cannot be controlled during the experiments.

3.5 Synthesis in Flow

3.5.1 Substrate Concentration Optimization

Three flow rates (0.1 mL/min, 0.25 mL/min, and 0.5 mL/min), three temperatures, (27.5 °C, 30 °C, and 32.5 °C), and three concentrations of AA and CAA (1.0 M and 0.5 M, 0.5 M and 0.25 M, 0.5 M and 0.5 M) were tested to optimize DERA-catalyze sequential aldol addition for statin side chain synthesis in continuous flow. Experimental set-up for continuous synthesis is described in Section 5.3 and sample analysis is outlined in Section 5.4.

The packed bed reactor (PBR) was the 20 cm × 0.8 cm HPLC column packed with lyophilized whole cells harboring DERA$_M$ immobilized in alginate matrix on loofa sponge (0.41 mg cells/ 1 g dry carrier). Different concentrations of acetaldehyde and chloroacetaldehyde were tested with three flow rates. The initial flowrate was set to 0.5 mL/min, at 60 minutes the flowrate was switched to 0.25 mL/min, and at 120 minutes into the reaction the flowrates was switched to 0.1 mL/min. Results are demonstrated in Figure 3.10.
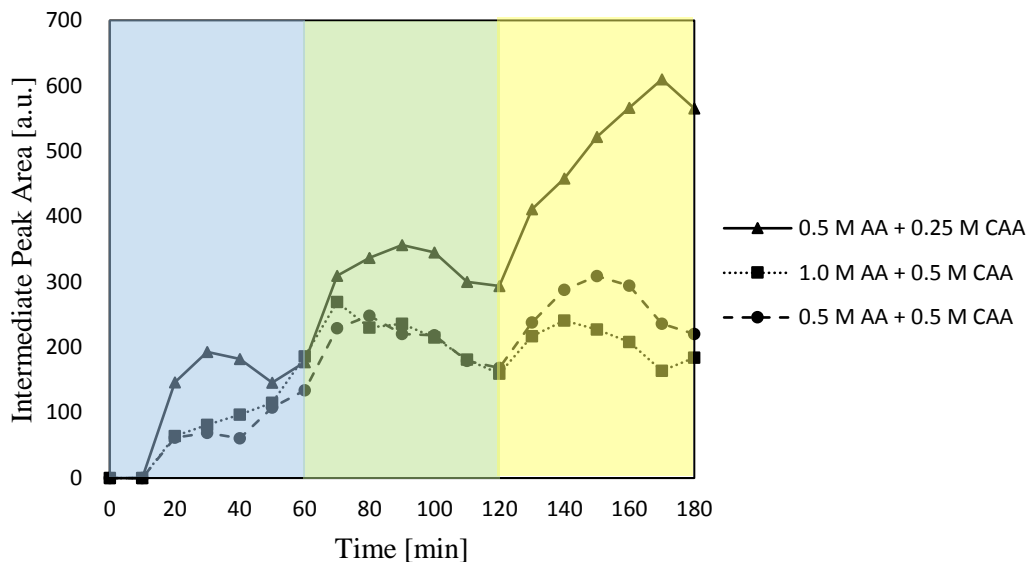
Figure 3.10: Test of the three concentrations of chloroacetaldehyde and acetaldehyde substrates for the DERA-catalyzed sequential aldol addition in flow at three flowrates (blue region=0.5 mL/min, green region=0.25 mL/min, yellow region=0.1 mL/min).

Higher reaction rates were observed with substrates of 0.5 M AA and 0.25 M CAA for all flowrates tested. The highest yield was achieved at $t = 170$ minutes with 0.1 mL/min flowrate. These findings agree with the batch experiments presented in Section 3.1. However, comparing the highest peak areas achieved, batch experiments yielded the CAA intermediate with a peak area 4.9 times larger than experiments in flow. Significant loss in enzyme activity is caused by the diffusional barrier created by the alginate matrix. Batch experiments (5 mL) performed by Bianca Grabner, M.Sc., with 100 mg of $DERA_M$ immobilized on loofa sponge using 1.0 M AA and 0.5 M CAA have shown a reaction progression 6 times slower than in batch experiments (5 mL) performed with 100 mg of free lyophilized enzyme and the same substrate concentration (data not shown). Additionally, experiments conducted by Stolarzewicz et al. showed reduced catalytic activity after immobilization of a lyophilized cell-bound lipase in alginate matrix [81]. Substrates have to first penetrate the matrix in order to reach the immobilized cells. Afterwards, substrates have to penetrate cell walls to reach the enzyme located in the cytoplasm while avoiding secondary enzymes. The reversed route is true for the formed reaction intermediates and products. Therefore, the required reaction time for converting the substrates into the desired products is much higher for a reaction utilizing an immobilized freeze-dried whole-cell biocatalyst compared to a reaction with a dispersed freeze-dried whole-cell biocatalyst.

A general trend of increasing reaction yield with decreasing flowrate is evident for all three reaction compositions analyzed. Even though high flowrates contribute to a better mixing and better external mass transfer, with the given constant reactor volume the residence time of reactants is too small to achieve full conversion (Table 3.4). The substrate concentration is maximized at the inlet of the packed bed reactor and decreases towards the outlet, eventually being equal to zero in ideal cases [82]. Increased flowrate lowers the concentration gradient leading to a larger amount of unreacted substrate in the reactor's bed. GC-FID analysis detected unreacted AA and CAA in all cases presented in Figure 3.10, however, the reaction peaks could not be quantified due to peak overlap, as discussed in Section 3.1.

Considering the substrate-induced inhibition, the reaction is more likely to be inhibited at a given reactor volume under higher flowrates and concentrations of the inhibitory substrates. In the present reaction, CAA and AA both inhibit $DERA_M$; however, CAA is the substrate currently with the most known inhibitory action in DERA-catalyzed aldol addition [27], [52]. The reaction of 0.5 M AA and 0.5 M CAA has the highest concentration of the unreacted AA due to the 1:1 molar ratio. The reaction composed of 1.0 M AA and 0.5 M CAA has the highest concentration of reactants in general. Mean residence time for experiments conducted under 0.5 mL/min and 0.25 mL/min are presented in Table 3.4, which are much lower than the mean residence time for the 0.1 mL/min flowrate. Low reaction yields for the reaction composed of 1.0 M AA and 0.5 M CAA and the reaction composed of 0.5 M AA and 0.5 M CAA are caused by short residence times that lead to an increased concentration of unreacted CAA and AA molecules and, as a consequence, $DERA_M$ inhibition. Therefore, substrate-induced inhibition has a considerable impact on batch and continuous DERA-catalyzed aldol addition reaction under the conditions tested.

The lowest flowrate tested allows for longest reaction time that the reactants spend in contact with the immobilized enzyme. The productivity of the 0.5 M AA and 0.5 M CAA slightly increased with the slower fluid flow. Due to side reactions, a limited amount of donor molecules is available to react with CAA, therefore leaving unreacted CAA available to cause enzyme inhibition. However, due to the longer residence time, no substrate accumulation, and lower overall substrate concentration of the feed, the observed inhibition is also lower compared to reaction with 1.0 M AA and 0.5 M CAA. Longer residence time caused by 0.1 mL/min flowrate (Table 3.4) seemed to have no impact on the enzyme inhibition, and thereby productivity, of the 1.0 M AA and 0.5 M CAA

reaction compared to results obtained with 0.25 mL/min flowrate experiment. This, perhaps, could be resolved by a reactor with larger length [82].

Reaction with substrate concentrations of 0.5 M AA and 0.25 M CAA was chosen for the in-flow temperature optimization experiments due to the highest reaction yields obtained and due to the less defined substrate-induced inhibition observed compared to the 0.5 M AA and 0.5 M CAA reaction and 1.0 M AA and 0.5 M CAA reaction (Figure 3.10).

3.5.2 Temperature Optimization

Three temperatures, 27.5 °C, 30 °C, and 32.5 °C, were tested for the in-flow DERA-catalyze aldol addition reaction under the three flowrates, 0.5 mL/min, 0.25 mL/min, and 0.1 mL/min. with 0.5 M AA and 0.25 M CAA substrates concentration. The tested temperatures were determined from the design of experiments (DoE) analysis previously performed by Bianca Grabner, M.Sc., in batch. Results from the continuous reaction performed at 27.5 °C, 30 °C, and 32.5 °C are demonstrated in Figure 3.11. Results from the continuous reaction performed at 32.5 °C are the same results presented in Figure 3.10 for the 0.5 M AA and 0.25 M CAA reaction.
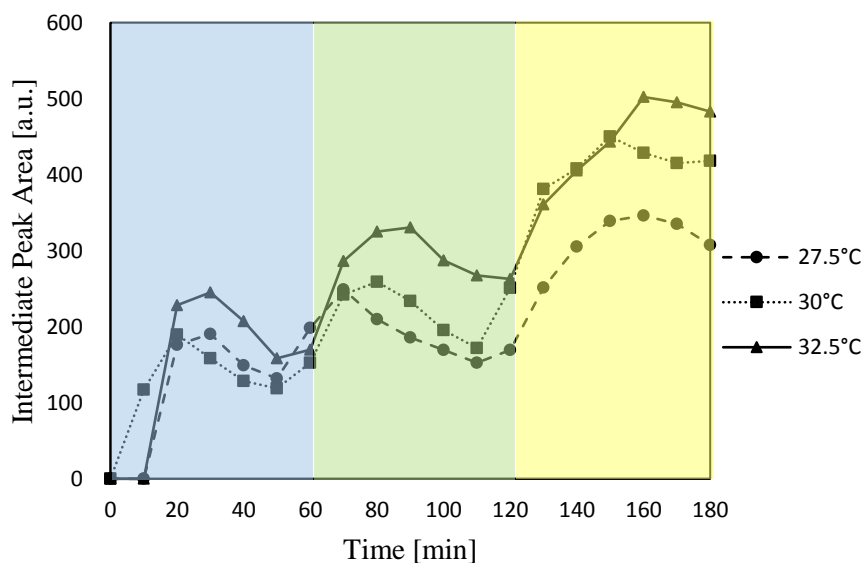
Figure 3.11: Temperature test showing intermediate peak areas of the DERA-catalyze sequential aldol addition with 0.5 M AA and 0.25 M CAA in flow at three flowrates (blue region=0.5 mL/min, green region=0.25 mL/min, yellow region=0.1 mL/min). The tested temperatures are 27.5 °C, 30 °C, and 32.5 °C.

An increase in enzyme activity with increasing temperature is evident in Figure 3.11 for all flowrates tested. Generally, the reaction rate increases with increasing temperature [35]. The

Brownian motion of the substrates is increased with increasing temperature, improving the likelihood of the substrates and the enzyme to collide. Additionally, the stability of the substrate bonds is reduced with increasing temperature, making them more inclined to break [35]. On the other hand, enzymes have optimum temperatures. Increasing the temperature past that point denatures the enzymes by disrupting tertiary structure [35]. As a consequence, an enzyme's activity is hindered, or the enzyme is completely deactivated. Temperatures lower than optimum decreases the motion of the molecules and atoms, which have a negative impact on protein flexibility [35]. Lowered protein flexibility lowers its activity. DERA showed higher activity at 32.5 °C when operated at neutral pH, which matches the results obtained by the DoE analysis in batch.

Similarly, to the in-flow experiments completed for substrate concentration optimization (Figure 3.10), the temperature experiments performed the best at 0.1 mL/min. The packed column is placed inside the plug & play reactor connected to a thermostat and due to the small reaction scale with packed reactor volume equal to ca. 6.1 mL and small flowrates, no considerable temperature gradients are assumed to be present [83]. Increased reaction productivity with decreased flowrate is attributed to the difference in residence times and internal mass transport (diffusion into alginate matrix pores), as discussed above.

RTD experiments have demonstrated a deviation from ideal plug flow behavior for 0.1 mL/min with D/uL values of 0.067 (Table 3.4). This indicates that back-mixing affects the reaction progression, however, the obtained dispersion number is most likely caused by the presence of molecular diffusion due to the low flowrate in addition to the random fluctuations outlined in Section 3.4. However, from the substrate concentration and temperature experiments, it can be concluded that aldol addition performed in continuous flow produces the highest amount of intermediate with the flowrate of 0.1 mL/min.

A packed bed reactor with a longer length will benefit the continuous synthesis process described in this work. First, a longer reactor will increase the residence time of the substrates and hence their contact with the biocatalyst. Additionally, for constant reaction conditions, the increased reactor length improves flow behaviour, with plug flow being more likely with sufficient reactor length [82].

Therefore, out of the conditions tested, the optimum conditions for the in-flow DERA-catalyzed sequential aldol addition reaction are 0.5 M AA and 0.25 M CAA, 0.1 mL/min flowrate, and a

reaction temperature of 32.5 °C. However, Figure 3.10 and Figure 3.11 show a slight decrease of the intermediate production for each flowrate region right before the flowrate change. This might be due to low alginate concentration used for immobilization that caused enzyme leaching [84]. Higher alginate concentration was investigated and results are presented in the next sub-section.

3.5.3 Alginate and DERA$_M$ Concentration Testing

Alginate concentration greatly impacts the physical properties of the calcium alginate matrix. High concentration of alginate increases the density of the immobilized matrix and minimizes leakage [70], [84]. Alginic salt concentration was increased to analyze the strength of the produced alginate matrix with standard DERA$_M$ concentration and with double DERA$_M$ concentration. Experimental procedure is described in Section 5.3 sample analysis is outlined in Section 5.4. Results are presented in Figure 3.12 below.
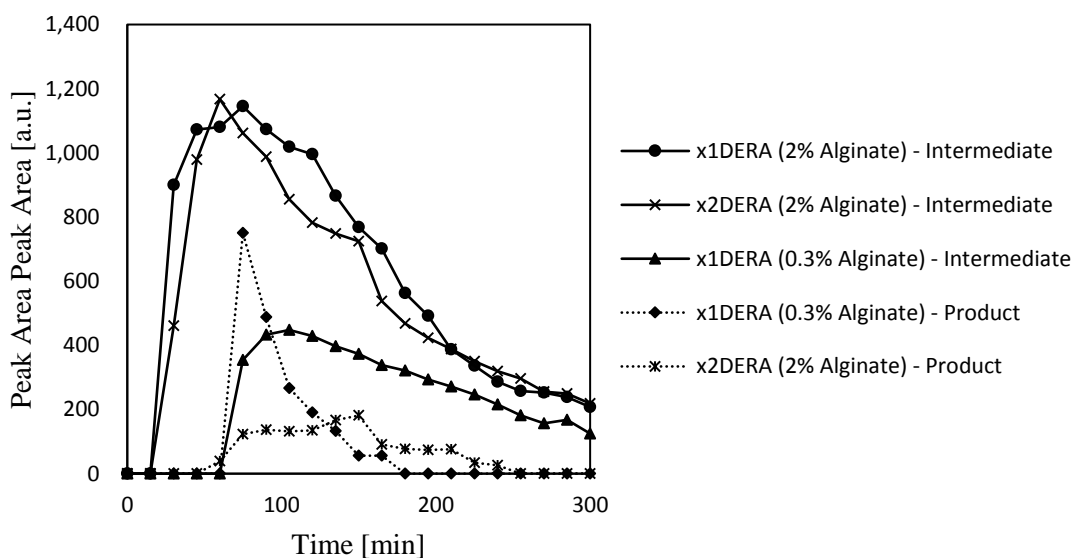
Figure 3.12: Intermediate and product peak areas of the DERA-catalyzed sequential aldol addition reaction in continuous settings with DERA$_M$ immobilized on loofa sponge with sodium alginate gel matrix composed of 0.3 % alginate and 2 % alginate. Different DERA$_M$ concentrations (standard – x1 DERA; double – x2 DERA) were tested for the alginate matrix composed of 2 % alginate.

DERA-catalyzed reaction with enzyme immobilized on loofa sponge in alginate matrix composed of 0.3 % alginate produced the lowest yields of the intermediate. A CAA product peak was detected starting with $t = 75$ minutes with an area of 750.83 a.u. (highest CAA product area detected). The last CAA product peak was detected at $t =$165 minutes with an area of 56.38 a.u. No difference in the intermediate production was observed for the reactions catalyzed by standard DERA$_M$

concentration and double DERA$_M$ concentration in the 2 % alginate matrix. However, x2 DERA$_M$ reaction started forming a CAA product at $t = 60$ minutes with a maximum peak area detected at $t = 150$ minutes with a value of 183.8 a.u. The areas of the product peaks were declining after that time point and were not detected past $t = 240$ minutes. The trend observed for the decline of the detected product peak areas resembles the decline of the detected intermediate peaks. The observed constant linear decline of the intermediate and product peak areas detected in the effluent stream of all concentrations of the biocatalyst and alginate tested might indicate enzyme wash off due to enzyme leaching.

The thickness and rigidity of the alginate matrix plays a crucial role in the observed reaction behavior. Increased alginate concentration improved the intermediate formation, however, the enzyme leaching was not avoided. Higher CAA product formation for the 0.3 % alginate experiment is most likely caused by easier penetration of substrates into the matrix and product into the reactor due to the thinner and weaker walls of the matrix. However, this also allows for a quicker biocatalyst wash off, as shown in Figure 3.12.

The reaction catalyzed by x2 DERA$_M$ concentration performed better than standard DERA$_M$ concentration with calcium alginate matrix composed of 2 % alginate. Despite the improved performance, it is hypothesized that the full potential of the double enzyme concentration was not reached due to the high viscosity of the alginate solution (prior to cross-linking) and increased thickness and decreased poor size of the cross-linked matrix caused by an increase in alginate concentration. High viscosity of the 2 % alginate solution made it difficult to disperse the lyophilized whole cells containing DERA$_M$. For the same reason, higher enzyme concentrations were not possible to achieve. The sponge soaks up the thick alginate-cell gel and the rest of the gel "coats" the sponge. Once the cross-linked matrix is made with calcium ions, only the cells closest to the inner surface of the alginate matrix are available for substrates due to the high thickness and density of the matrix. Therefore, the enzyme located closest to the sponge or inside its void spaces is partially or completely unavailable to its substrates.

Possibility of the enzyme wash off makes the DERA$_M$ concentration testing results incomparable to the batch experiments (Figure 3.7). However, in both schemes, a well-defined limit of the lyophilized cell concentration exits because high concentrations hinder mass transport and thereby

reduce reaction yields. An enzyme leaching test was performed to verify the release of enzyme into the reaction media. Results are presented in sub-section below.

3.6 Enzyme Leaching

Experimental set-up of enzyme leaching experiment is described in Section 5.8. Reaction progress was monitored by GC-FID following the procedure described in Section 5.4. The peak areas of the reaction samples analyzed immediately after collection from the reactor (0 hours) and analyzed after overnight storage (24 hours) were compared. The results are presented in Table 3.5 below.

Table 3.5: GC-FID peak areas of the intermediate, product, and side products of the DERA-catalyzed aldol addition detected for samples collected from the reactor effluent stream (0 hours) and samples of the effluent stream left overnight (24 hours).

Sample Time [min]	60 minutes			90 minutes		
	Intermediate	**Product**	**Side Products**	**Intermediate**	**Product**	**Side Products**
0 hours	1,535.85	0	187.65	754.43	874.05	724.46
24 hours	1,310.26	0	321.05	1,412.21	870.87	848.97

The sample taken at $t = 60$ minutes showed a 71.1 % increase in the total area of side product peaks detected after overnight storage compared to analysis performed immediately after sample collection. Intermediate peak area of the same sample has decreased by 14.7 % after the sample was stored overnight. The increase in side products formation might be caused by the observed consumption of the intermediate formed and by the unreacted CAA and AA present in solution available for side reactions. This suggests that the enzyme is present in the sample.

The sample taken at $t = 90$ minutes has an increase of 87.2 % in the area of intermediate peak. Additionally, the total area of the side product peaks increased by 2.9 %. The decrease in product peak area over night is considered to be caused by instrument sensitivity and thereby insignificant. A drastic increase in intermediate formation overnight indicates the presence of the enzyme in the sample.

Both of the time points tested have demonstrated signs of the enzyme present inside the samples of the reaction mixture collected at the effluent of the packed column confirming that the immobilized system leaches the biocatalyst. Additionally, sample taken at $t = 90$ minutes shows

bigger changes to the peak areas compared to the sample taken at $t = 60$ minutes, indicating an increased amount of enzyme leached out of the reactor with time. This corresponds to the linear decrease in the detected intermediate over time shown in Figure 3.12 because less enzyme is available as the reaction progresses.

The enzyme leaching observed in Figure 3.12 and Table 3.5 might be caused by several factors. First, the loofa sponge covered with calcium alginate matrix is too thick to freely be placed inside the column and thinner cylinders of loofa sponge are impossible to cut manually. Therefore, the packing technique utilizes a small spatula for inserting the loofa sponge into the column. This process can disrupt the matrix if too much force is applied during packing and when the spatula is taken out of the column. The disrupted surface of the matrix exposes the cells to the reaction mixture. Secondly, the shear stress exerted on the surface of the immobilized support by the flowing reaction solution inside the column might slowly disrupt the alginate matrix even at low flowrates. This gradually thins the layer of alginate matrix releasing lyophilized cells into the surrounding media. Thirdly, only L-guluronate (G) residues of alginate involve in cross-linking with divalent cations and alginate with the lowest M/G ratio forms more rigid and porous gels [70], [85]. However, the manufacturer did not provide the residue ratio and therefore it is possible for the alginate matrix to have a lower strength due to higher M/G ratio. Lastly, lyophilized whole cells do not dissolve in an aqueous media and create an additional phase. When sodium alginate gel with dispersed lyophilized pellets is placed in the calcium chloride solution for gelation, the lyophilized cell pellets might interfere with the ionic bond formation. This might lead to less ionic bonds formed or uneven distribution of the ionic bonds and thereby weaker alginate matrix.

Additional factors, such as cross-linking solution type, cross-linking solution strength (divalent cation strength), gelation time, and, as mentioned above, alginate concentration play a role in the quality of the produced alginate matrix [70], [84]. However, limited long-term stability of the ionically-cross linked alginate matrices due to the interaction of the released divalent ions and monovalent cations of the surrounding media is a well-known disadvantage [66]. Therefore, finding the appropriate formulation for the required reaction conditions is crucial for achieving the desired results.

4 Conclusion and Future Recommendations

4.1 Conclusion

Statins are effective therapeutics prescribed to lower the risk of cardiovascular disease, the leading cause of death in the world [1]. The required chemical and stereochemical purity of statins is difficult to achieve in chemical synthesis, so the pharmaceutical industry is interested in investigating applications of biotransformation processes in the synthesis of statin building blocks [6], [8]. Furthermore, continuous manufacturing has been heavily researched and progressively implemented in the pharmaceutical industry for various drug types [11], [12], [61]. The purpose of this master's thesis was to investigate the DERA-catalyzed step in statin side chain synthesis and its potential to be performed as a continuous process.

According to the current literature, DERA-catalyzed sequential aldol addition reaction has not been performed with lyophilized whole cells harboring the C47M DERA (DERA$_M$) mutant. Therefore, different aldehyde substrates were screened in batch to assess their performance with lyophilized whole cells and therefore, the activity of DERA$_M$ inside cells. Chloroacetaldehyde was chosen as an acceptor molecule for further in-flow DERA-catalyzed aldol addition. Although acetaldehyde had higher yield of the desired product, chloroacetaldehyde is known to be a potent DERA inhibitor. This makes it an interesting substrate for an in-flow synthesis because it allows to see the effect of continuous set-up on DERA-catalyzed reaction behavior with an inhibitor compared to batch.

The intermediate and lactol product generated by the lyophilized whole-cell DERA-catalyzed sequential aldol addition using acetaldehyde as donor and chloroacetaldehyde as acceptor were characterized. However, the intermediate and product calibration yielded inconsistent results and were unsuccessful because of the reaction scale limitations, low production rates, and oily nature of the purified substances. Therefore, the reaction progression and product formation in batch and continuous flow were quantified by the GC-FID peak areas.

Prior to beginning the synthesis in continuous set-up, preliminary packed bed reactor (PBR) performance was evaluated. Mean residence times and the dispersion numbers, D/uL, for three

flowrates were experimentally determined by executing Residence Time Distribution (RTD) experiments. This evaluation demonstrated deviations from ideal plug flow behavior in all reaction set-ups tested. The choice of the solid support for biocatalyst immobilization and reactor packing procedure were the main factors for random fluctuations that induced back mixing.

Following the RTD experiments, the optimum parameters were determined for the DERA-catalyzed sequential aldol addition reaction executed continuously. The optimization of initial molar concentration of substrates, reaction mixture flowrate, and reaction temperature were performed and yielded the following results: 0.5 M acetaldehyde and 0.25 M chloroacetaldehyde, 0.1 mL/min, and 32.5 °C. Reaction yields obtained from the continuous set-up were considerably lower than the yields of batch reactions. Limited reactor length available was one of the factors that affected the reaction yields.

Enzyme immobilization played the most significant role in the unsatisfactory reaction performance. The alginate matrix used to immobilize lyophilized cells-containing DERA$_M$ created an additional transport barrier for substrates before reaching the biocatalyst. Furthermore, the packing method disrupted the alginate matrix, releasing lyophilized cell powder to the reaction stream. This caused a rapid decrease of the biocatalyst availability inside the reactor and hence decreased the reaction yield. An enzyme leaching experiment confirmed the biocatalyst presence in the reactor effluent stream.

Despite the low yields obtained with the continuous set-up, this study demonstrated the limitations of performing DERA-catalyzed sequential aldol addition reaction in flow. After addressing reactor length and enzyme immobilization, there is a possibility that the improved continuous set-up will be useful in industry to increase the chemical and stereochemical purity of synthesized statins.

4.2 Future Recommendations

The work presented here demonstrated that continuously synthesized lactol by DERA-catalyzed sequential aldol addition reaction is a promising procedure for statin side chain synthesis. However, further research is necessary to reach appropriate production yields. The proposed improvements include an increased reactor length, utilization of cell lysate for reactions, and replacing loofa sponge solid support with chitosan/alginate beads.

As seen from the results of continuous experiments, the first lactol peak is detected when the reaction time approaches the mean residence time for the reaction with optimum conditions ($\bar{t}_{exp} = 62.7$ minutes). A longer reactor length will increase the amount of time intermediate molecules spend in contact with the biocatalyst for further product formation.

Whole-cell biocatalysis has many advantages such as simplicity of handling and protection of the enzyme by cell membrane [38]. However, the results of this work and work conducted by Stolarzewicz et al. with a different enzyme have demonstrated a decrease in enzyme activity for freeze-dried whole cells immobilized in alginate [81]. Lyophilized whole cells containing DERA is a good way to store the biocatalyst. However, it is proposed to use cell lysate for the aldol addition reaction, which can be obtained from the lyophilized cell powder when required. This will decrease the encountered mass transport limitations once the enzyme is immobilized without additional purification steps.

Loofa sponge is readily available, environmentally friendly, and a cost-efficient solid support for enzyme immobilization [68]. One of the main disadvantages of loofa sponge was the difficulty of packing the material inside a long tubular reactor, such as a packed bed reactor, without disrupting the immobilized matrix coating the sponge. It is proposed to immobilize DERA in alginate beads to simplify reactor packing procedure and avoid alginate matrix disruption and thereby enzyme leaching.

The alginate polymer formulation should also be optimized to reach appropriate bead rigidity and porosity. First, alginate of a known ratio of mannuronic and guluronic residues should be used because physical and chemical properties of alginate matrix are affected by the composition and sequence of mannuronic and guluronic residues [70], [86]. The size, shape, porosity, and rigidity of the alginate beads depend on alginate concentration, cross-linking solution concentration and strength, and cross-linking time. A polycation such as chitosan should be added to the formulation because polycations stabilize the matrix in presence of calcium cross-linking solutions [86], [87]. Therefore, optimizing the alginate concentration, cross-linking solution and its strength, and adding chitosan to the gel will rid of the leaching issue by increasing alginate beads stability.

5 Materials and Methods

A detailed description of the experimental methods employed to obtain the presented results is outlined below. All of the chemical compounds used during the experiments are listed in Table 5.2 along with their relevant information. This table does not include material used for the outsourced experiments.

5.1 Expression of DERA in *E. coli* BL21 (DE3)

An expression plasmid, pET21a_deOC_EC_C47M_6xhis, containing C47M DERA mutant gene was provided by Jörg Pietruszka, Ph.D., Research Center Jülich, Germany. Anna Schweiger at the Institute of Molecular Biotechnology, TU Graz, completed and provided the C47M DERA expression protocol.

A 5 mL of LB solution containing 100 µg/mL ampicillin was inoculated with *E. coli* BL21 (DE3) cells harboring the DERA-coding gene in a pET21a-vector. The inoculated media was incubated at 37 °C under shaking at a speed of 130 rpm overnight. The entire ONC was used to inoculate 400 mL of TB medium containing 100 µg/mL ampicillin in 2 L baffled shake flasks. The resultant main culture was incubated at 37 °C under shaking at a speed of 120 rpm until 0.5-0.8 OD600 was reached.

Overexpression was induced by addition of 0.1 mM IPTG, following an incubation under shaking at 120 rpm and 25 °C for 16 hours. After 16 hours of incubation, the cells were centrifuged for 15 minutes at 7000×g and 4 °C. The harvested cells were then washed by resuspension in 40 mL of 20 mM pH 7 phosphate buffer. The cells were centrifuged for 15 minutes at 4000 rpm and 4 °C and the pellets were freeze-dried.

SDS-PAGE

The freeze-dried cells were resuspended in 20 mM pH 7.0 Phosphate buffer and a suitable aliquot (7/OD) was taken. The respective pellets were treated with BugBuster® and the soluble and insoluble fractions were analyzed separately on the SDS-Gel to assess extent of expression.

5.2 Substrates

Acetaldehyde, chloroacetaldehyde, acrolein, cinnamaldehyde, and benzaldehyde were screened as substrates of DERA in batch for further applications in continuous flow experiments. These substrates and their molecular structure are listed in Table 3.1. For further information on the compounds, refer to Table 5.2.

5.3 Batch, Fed-Batch, and Continuous Reactions

5.3.1 Batch Reaction

The optimal reaction temperature and pH were determined to be 32.5 °C and 7.5, respectively, for the DERA-catalyzed sequential aldol reaction by Bianca Grabner, M.Sc., in previous experiments.

0.1 M pH 7.5 TEOA buffer was heated to 32.5 °C with constant stirring. DMSO was added to the buffer to make a final concentration of 1.4 % v/v. Lyophilized C47M mutant whole cells were suspended in the solution to a desired concentration. The tested freeze-dried cell concentrations were 2 mg/mL, 10 mg/mL, 20 mg/mL, 40 mg/mL, and 80 mg/mL. The acceptor aldehyde was added to the reaction mixture, followed by the addition of anhydrous acetaldehyde (the donor). The tested molar ratio of donor:acceptor were 0.5:0.5, 1.0:0.5, and 0.5:0.25. The solution was stoppered and maintained at 32.5 °C with continuous stirring. The reaction volumes tested were 50 mL, 5 mL, 1 mL, and 0.5 mL. Several reaction times were analyzed.

5.3.2 Fed-Batch Reaction

Fed-batch reaction was performed based on the protocol described by Ručigaj A. and Krajnc M. [49]. The enzyme suspension (0.1 M pH 7.5 TEOA buffer, 1.4 % v/v DMSO, and

lyophilized cells) preparation and the reaction conditions were identical to the batch reaction. Chloroacetaldehyde (acceptor) and acetaldehyde (donor) were used as substrates for the fed-batch reaction. Both substrates were added to the enzyme suspension of 5 mL initial volume continuously by the polyvalent programmable syringe pumps (Lambda Laboratory Instruments, VIT-FIT) at different rate. Each pump was equipped with one 20 mL syringe. The syringes were filled with either donor or acceptor in 0.1 M pH 7.5 TEOA buffer at an initial concentration of 2.8 M and 1.8 M, respectively.

For 120 minutes of the fed-batch reaction, chloroacetaldehyde and/or acetaldehyde were added to the enzyme suspension at various rates as described in Table 5.1. After feeding, the reaction was left to proceed for an additional hour. The total reaction time was 3 hours and the final volume of the reaction mixture was 9 mL.

Table 5.1: Fed-batch reaction regime of acetaldehyde (donor) and chloroacetaldehyde (acceptor) feeding.

Feeding Time [min]	Feeding Rate [mL/hr]		Amount Fed [mmol]		Final Concentration [mol/L]	
	Donor	Acceptor	Donor	Acceptor	Donor	Acceptor
0-30	2.6	2.9	3.7	2.5	0.50	0.33
30-60	0.9	0.0	1.3	0.0	0.64	0.32
60-120	0.8	0.0	2.0	0.0	0.83	0.29

5.3.3 Continuous Reaction

The set-up for continuous DERA-catalyzed aldol reaction included the plug & play reactor, a Lauda P18 Proline thermostat, a 20 cm × 0.8 cm HPLC column packed with biocatalyst, an HPLC pump (Knauer, Azura P4.1 S), and a vessel with reaction mixture [83]. All of the set-up components were connected by capillary tubes. A scheme of the set-up is shown in Figure 5.1 below.
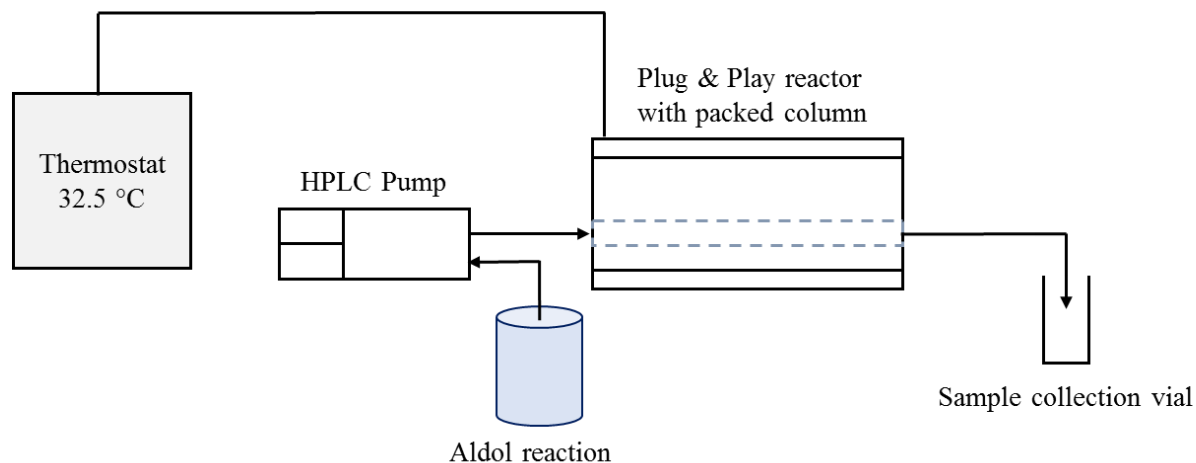
Figure 5.1: Experimental set-up for DERA-catalyzed aldol reaction carried out in continuous flow.

Two pieces of carrier (loofa sponge; Croll & Denecke GmbH) with immobilized enzyme were inserted into 20 cm × 0.8 cm HPLC column by using a thin spatula. The biocatalyst immobilization technique used to immobilize DERA on loofa sponge for continuous flow experiments is described in Section 5.7. The column was connected to the HPLC pump and flushed vertically with 0.1 M pH 7.5 TEOA buffer at 1.0 mL/min – 3.0 mL/min to get rid of air bubbles. Then, the column was placed in the pre-heated plug & play reactor and allowed to equilibrate at the initial experimental flowrate for 30 minutes [83]. The reaction mixture (0.1 M pH 7.5 TEOA with 1.4 % v/v DMSO, and both substrates) was prepared as described in the batch reaction section without the enzyme addition. Immediately after addition of donor aldehyde, the reaction mixture was connected to the HPLC pump, the reaction vessel opening was sealed with parafilm, and the HPLC pump head was flushed and the reaction mixture was pumped through the reactor.

5.4 Sample Analysis

5.4.1 Gas Chromatography

When acceptor molecules were acetaldehyde, chloroacetaldehyde, or acrolein, the reaction-mixture samples were analyzed with gas chromatography. 200 µL reaction-mixture samples were quenched with 4 vol. MeCN and centrifuged for 10 minutes at 20 °C and 10,000 rpm. 700 µL of the supernatant was transferred to GC vials for analysis.

Analysis was performed on a PerkinElmer Clarus 500 Gas Chromatography (GC) system equipped with flame ionization detector (FID). The column used was Machery-Nagel Optima-5 MS capillary column (320 µm inner diameter and 0.25 µm film coating). N_2 was used as carrier gas. Sample injection volume was 1.0 µL. The flow rates were 45 mL/min H_2 and 450 mL/min synthetic air; initial temperature was held at 50 °C for 5 minutes and the gradient of 10 °C/min was applied until 250 °C was reached and held for 5 minutes. The intermediate and product peaks were identified by using nuclear magnetic resonance (NMR) in previous experiments performed by Bianca Grabner, M.Sc.

5.4.2 Reverse Phase HPLC

When aromatic acceptor substrates were used (benzaldehyde or cinnamaldehyde), the reaction-mixture samples were analyzed with HPLC. 200 µL reaction-mixture samples were quenched with 4 vol. MeCN and centrifuged for 10 minutes at 20 °C and 10,000 rpm. 100 µL of the supernatant was diluted with 1 mL of solvent (30 % MeOH and 70 % phosphate buffer) for analysis.

The samples were analyzed with a reversed phase high-performance liquid chromatography (RP-HPLC) on an Agilent 1100 system equipped with a ThermoFischer Scientific Accucore^{TM} C-18 column (50×4.6 mm; 2.6 µm). 2 µL of sample were injected and analyzed at 25 °C. A 30 % MeOH and 70 % phosphate buffer mobile phase was used with a flowrate of 1.0 mL/min. A UV detector was used for analyte detection. The phosphate buffer was prepared by mixing 300 mL ultrapure H_2O and 1 mL of phosphoric acid solution (85 wt. % in H_2O).

5.4.3 Crystalline

The phases present in the aldol reactions involving aromatic acceptor molecules were investigated with Crystalline (Technobis). The reaction mixture was prepared as described in Section 5.3 for batch reactions without the biocatalyst addition. Temperature was set to 32.5 °C and bottom stirring was set to 1,000 rpm. Bitmap images were captured every second for 120 minutes.

5.5 Intermediate and Product Purification

The purification procedure steps were executed according to procedure outlined by Ošlaj et al. with slight modifications [72]. The purification procedure was optimized and tailored to account for the differences between the reaction conditions.

Intermediate and product purified were synthesized in batch and fed-batch, respectively. The reaction flask was removed from heat after 5 minutes for the batch reaction and 180 minutes for the fed-batch reaction. 3 vol. acetone was added to the reactions, stoppered, and left standing at room temperature for 30 minutes. The mixture was then filtered by gravity filtration using a fluted filter paper for enzyme capturing. Acetone was evaporated under reduced pressure and the enzyme-free reaction mixture was extracted 3 times with 2 vol. EtOAc. The organic EtOAc phases were collected, dried over $MgSO_4$, and filtered with fluted filter paper. After EtOAc evaporation under reduced pressure, intermediate and/or product were obtained as a light brown-yellow oil.

5.6 Residence Time Distribution

An HPLC column (20 cm $\times$ 0.8 cm) packed with loofa sponge was connected to two HPLC pumps (Knauer, Azura P4.1 S) flushed with either solvent or tracer. The outlets of the HPLC pumps and the inlet of the column were connected via a 6-port injection valve (IDEX Health & Science LLC, V-450) used for efficient solvent switching during a step input. The column was placed inside the plug & play reactor connected to a Lauda P18 Proline thermostat [83]. The tracer signal was detected by an inline UV-vis flow cell (Avantes, Cell-Z-10) with 10 mm optical path length at the outlet of the reactor. UV-vis measurements were performed with an Avantes system equipped with a detector (Avantes, AvaSpec-ULS2048) and a deuterium lamp (Avantes, AvaLight-DS-DUV) light source. The RTD set-up is shown in Figure 5.2.
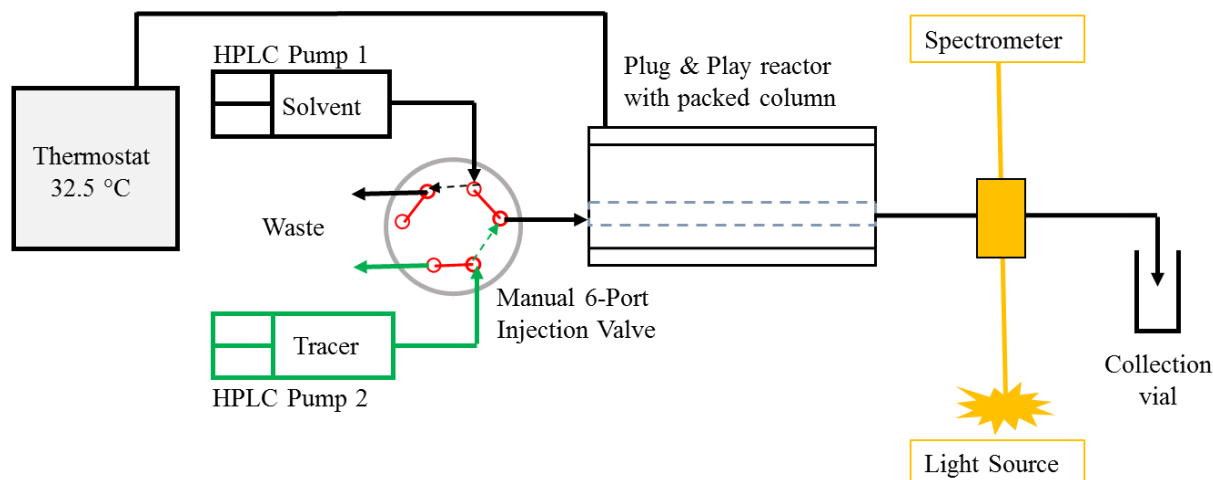
Figure 5.2: Experimental set-up for the RTD determination in flow. The step input is made by switching the manual 6-port injection valve from HPLC Pump 1 (Solvent) to HPLC Pump 2 (Tracer) position, allowing a constant flow of tracer through the column and subsequently the flow cell.

Loofa sponge was soaked in 0.9 % w/v NaCl buffer for one hour. The HPLC column was packed with the soaked loofa sponge and connected to an HPLC pump flushed with 60 % v/v EtOH in H_2O (RTD solvent). The column was flushed vertically with the RTD solvent to get rid of air bubbles. The column was placed inside the plug & play reactor and connected to the UV-vis flow cell with Avantes system [83]. Both pumps were set to identical flowrates of either 0.5 mL/min, 0.25 mL/min, or 0.1 mL/min. After equilibration to a constant signal, a baseline correction was performed by measuring the absorption at 500 nm- 506 nm wavelength. The flow to the column was switched from RTD solvent to tracer (0.4 % v/v anisole in RTD solvent) manually with the 6-port injection valve for the step input. The tracer absorption was measured at 268 nm- 274 nm wavelength. Detected signal values were saved every 500 ms.

Theoretical mean residence time, $\bar{t}_{th}$, was calculated by the following equation:

$$\bar{t}_{th} = \frac{(V_R - V_S)}{v} \tag{5.1}$$

where V_R is the empty reactor volume in mL, V_S is the volume of the loofa sponge soaked in RTD solvent (EtOH) in mL, and v is the flow velocity in mL/min. Volume of a loofa sponge was determined by applying the Archimedes' principle. A loofa sponge was placed in graduated cylinder filled with water and the volume of the displaced water was read from the graduated cylinder marks. Soaked loofa sponge was used to account for the sponge expansion.

5.7 Enzyme Immobilization

Loofa sponge was cut to completely be packed into the 20 cm × 0.8 cm HPLC column. The amount of NaCl buffer and freeze-dried cells required was determined by weight of the dry loofa sponge – 8 mL NaCl/ 1 g dry carrier and 0.41 mg cells/ 1 g dry carrier. The immobilization process is illustrated in Figure 5.3. Aqueous sodium alginate solution was prepared by dissolving alginic acid sodium salt (alginate) in 0.9 % w/v NaCl buffer to either 0.3 % w/v or 3 % w/v (Figure 5.3 (a)). Freeze-dried DERA cells were suspended in the prepared sodium alginate solution forming a viscous yellow gel-like mixture used for soaking the loofa sponge cut segments (Figure 5.3 (a)). After completely soaking up the entire DERA-alginate solution, loofa sponge was submerged into 2 % w/v CaCl$_2$ for 1 hour with stirring at room temperature for cross-linking, followed by 30 minutes of air-drying (Figure 5.3 (b)). The resultant loofa sponge carrying immobilized freeze-dried whole cells entrapped by alginate was used to pack the HPLC column for further use in continuous flow experiments.
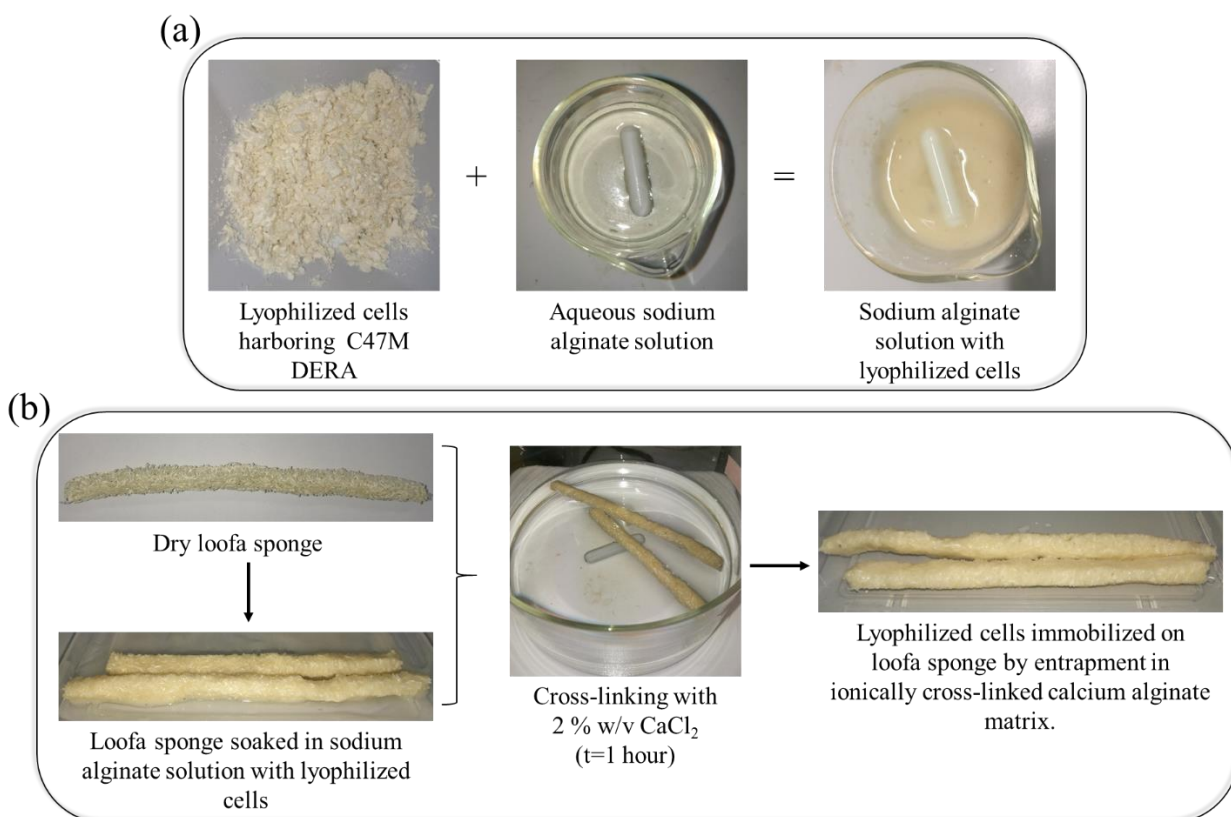
Figure 5.3: Immobilization of the lyophilized cells harboring C47M DERA mutant illustrating (a) preparation of the sodium alginate solution with the lyophilized cells and (b) cross-linking after soaking the sponge in the sodium alginate solution with the lyophilized cells and the final immobilized product.

5.8 Enzyme Leaching

Enzyme leaching experimental set-up was identical to the continuous set-up described in Section 5.3 above and illustrated in Figure 5.1 with a minor modification in sample analysis. Reaction samples were taken at t = 0 minutes, 30 minutes, 60 minutes, and 90 minutes. Samples of each time point were split into two batches. One of the sample batches was immediately prepared for GC-FID sample analysis as described in Section 5.4, whereas the second sample batch was left overnight at room temperature without MeCN addition. The overnight samples were analyzed the next day with GC-FID sample preparation and analysis described in Section 5.4. The intermediate, product, and side products GC-FID peak areas of both sample batches were compared at the time points tested and analyzed for enzyme leaching.

Table 5.2: Chemical compounds used during the experimental work and their relevant information.

Compound Common Name	Chemical Formula	MW [g/mol]	Company	CAS Number	Additional Information
Acetaldehyde	C_2H_4O	44.05	Sigma-Aldrich	75-07-0	$\geq 99.5\ \%$ $\rho = 0.785$ g/mL
Acetone	C_3H_6O	58.08	Fisher Scientific	67-64-1	Analytical reagent grade
Acetonitrile (MeCN)	C_2H_3N	41.05	Carl Roth	75-05-8	--
Acrolein	C_3H_4O	56.06	Sigma Aldrich	107-02-8	$\rho = 0.839$ g/mL
Alginate (alginic acid sodium salt)	$(C_6H_8O_6)n$	N/A	Carl Roth	9005-38-3	--
Anisole	C_7H_8O	108.13	Merck Millipore	100-66-3	$\rho = 0.994$ g/mL
Benzaldehyde	C_7H_6O	106.12	Sigma-Aldrich	100-52-7	$\rho = 1.04$ g/mL
Calcium Chloride Dihydrate	$CaCl_2 \cdot 2H_2O$	147.01	Sigma-Aldrich	10035-04-8	--
Chloroacetaldehyde	C_2H_3ClO	78.50	Sigma-Aldrich	107-20-0	~50 wt. % in H_2O $\rho = 1.236$ g/mL
trans-Cinnamaldehyde	C_9H_8O	132.16	Sigma-Aldrich	14371-10-9	99 % $\rho = 1.05$ g/mL
Dichloromethane	CH_2Cl_2	84.93	Carl Roth	75-09-2	$\geq 99.5\ \%$
Dimethyl Sulfoxide (DMSO)	C_2H_6OS	78.13	Sigma-Aldrich	67-68-5	$\geq 99.9\ \%$
Ethanol (EtOH)	C_2H_6O	46.07	Carl Roth	64-17-5	$\geq 96\ \%$
Ethyl Acetate (EtOAc)	$C_4H_8O_2$	88.106	Chem-Lab	141-78-6	$\geq 99.5\ \%$
Magnesium Sulfate	$MgSO_4$	120.37	Sigma-Aldrich	7487-88-9	Anhydrous $\geq 98\ \%$
Methanol (MeOH)	CH_4O	32.04	Honeywell	67-56-1	HPLC grade $\geq 99.9\ \%$
Phosphoric acid solution	H_3PO_4	98.00	Sigma-Aldrich	7664-38-2	85 wt. % in H_2O

Compound Common Name	Chemical Formula	MW [g/mol]	Company	CAS Number	Additional Information
Sodium Chloride	NaCl	58.44	Carl Roth	7647-14-5	$\geq$ 99.5 %
Triethanolamine (TEOA)	$C_6H_{15}NO_3$	149.19	Merck Millipore	102-71-6	$\geq$ 99 % ρ = 1.12 g/mL

6 Bibliography

[1]   The top 10 causes of death. (2018). Retrieved May 5, 2019, from https://www.who.int/news-room/fact-sheets/detail/the-top-10-causes-of-death

[2]   Cardiovascular diseases (CVDs). (2017). Retrieved May 5, 2019, from https://www.who.int/news-room/fact-sheets/detail/cardiovascular-diseases-(cvds)

[3]   Ischemic Heart Disease. (n.d.). Retrieved May 5, 2019, from https://www.nhlbi.nih.gov/health-topics/ischemic-heart-disease

[4]   Raised cholesterol. (2015, March 27). Retrieved May 5, 2019, from https://www.who.int/gho/ncd/risk_factors/cholesterol_text/en/ (accessed on 05.05.2019)

[5]   Davies, J. T., Delfino, S. F., Feinberg, C. E., Johnson, M. F., Nappi, V. L., Olinger, J. T., … Swanson, H. I. (2016). Current and Emerging Uses of Statins in Clinical Therapeutics: A Review. *Lipid Insights*, *9*. doi: 10.4137/lpi.s37450

[6]   Hoyos, P., Pace, V., & Alcántara, A. (2019). Biocatalyzed Synthesis of Statins: A Sustainable Strategy for the Preparation of Valuable Drugs. *Catalysts*, *9*(3), 260. doi: 10.3390/catal9030260

[7]   Kane, S. P. (n.d.). The Top 200 Drugs of 2019. Retrieved May 8, 2019 from https://clincalc.com/DrugStats/

[8]   Müller, M. (2005). Chemoenzymatic Synthesis of Building Blocks for Statin Side Chains. *Angewandte Chemie International Edition*, *44*(3), 362–365. doi: 10.1002/anie.200460852

[9]   Tao, J., & Xu, J.-H. (2009). Biocatalysis in development of green pharmaceutical processes. *Current Opinion in Chemical Biology*, *13*(1), 43–50. doi: 10.1016/j.cbpa.2009.01.018

[10]   Sakuraba, H., Yoneda, K., Yoshihara, K., Satoh, K., Kawakami, R., Uto, Y., … Ohshima, T. (2007). Sequential Aldol Condensation Catalyzed by Hyperthermophilic 2-Deoxy-D-Ribose-5-Phosphate Aldolase. *Applied and Environmental Microbiology*, *73*(22), 7427–7434. doi: 10.1128/aem.01101-07

[11]   Adamo, A., Beingessner, R. L., Behnam, M., Chen, J., Jamison, T. F., Jensen, K. F., … Zhang, P. (2016). On-demand continuous-flow production of pharmaceuticals in a compact, reconfigurable system. *Science*, *352*(6281), 61–67. doi: 10.1126/science.aaf1337

[12]   Lee, S. L., O'Connor, T. F., Yang, X., Cruz, C. N., Chatterjee, S., Madurawe, R. D., … Woodcock, J. (2015). Modernizing Pharmaceutical Manufacturing: from Batch to Continuous Production. *Journal of Pharmaceutical Innovation*, *10*(3), 191–199. doi: 10.1007/s12247-015-9215-8

[13]   Kleinebudde, P., Khinast, J. G., & Rantanen, J. (2017). *Continuous manufacturing of pharmaceuticals*. Hoboken, NJ: Wiley

[14]   Britton, J., Majumdar, S., & Weiss, G. A. (2018). Continuous flow biocatalysis. *Chemical Society Reviews*, *47*(15), 5891–5918. doi: 10.1039/c7cs00906b

[15]   Thompson, M. P., Peñafiel, I., Cosgrove, S. C., & Turner, N. J. (2018). Biocatalysis Using Immobilized Enzymes in Continuous Flow for the Synthesis of Fine Chemicals. *Organic Process Research & Development*, *23*(1), 9–18. doi: 10.1021/acs.oprd.8b00305

[16]   Casar, Z. (2010). Historic Overview and Recent Advances in the Synthesis of Super-statins. *Current Organic Chemistry*, *14*(8), 816–845. doi: 10.2174/138527210791111858

[17]   Stossel, T. P. (2008). The Discovery of Statins. *Cell*, *134*(6), 903–905. doi: 10.1016/j.cell.2008.09.008

[18]   Endo, A. (2010). A historical perspective on the discovery of statins. *Proceedings of the Japan Academy, Series B*, *86*(5), 484–493. doi: 10.2183/pjab.86.484

[19]   Endo, A. (2004). The discovery and development of HMG-CoA reductase inhibitors. *Atherosclerosis Supplements*, *5*(3), 67–80. doi: 10.1016/j.atherosclerosissup.2004.08.026

[20]   Berg, J. M., Tymoczko, J. L., Stryer, L., & Stryer, L. (2002). *Biochemistry* (5th ed.). New York: W.H. Freeman

[21]   Istvan, E. S. (2001). Structural Mechanism for Statin Inhibition of HMG-CoA Reductase. *Science*, *292*(5519), 1160–1164. doi: 10.1126/science.1059344

[22]   Smith, S. W. (2009). Chiral Toxicology: Its the Same Thing…Only Different. *Toxicological Sciences*, *110*(1), 4–30. doi: 10.1093/toxsci/kfp097

[23]   Patel, R. N. (2017). Biocatalysis for synthesis of pharmaceuticals. *Bioorganic & Medicinal Chemistry*, *26*(7), 1252–1274. doi: 10.1016/j.bmc.2017.05.023

[24]   Liljeblad, A., Kallinen, A., & Kanerva, L. (2009). Biocatalysis in the Preparation of the Statin Side Chain. *Current Organic Synthesis*, *6*(4), 362–379. doi: 10.2174/157017909789108738

[25]   Brooks, W. H., Guida, W. C., & Daniel, K. G. (2011). The Significance of Chirality in Drug Design and Development. *Current Topics in Medicinal Chemistry*, *11*(7), 760–770. doi: 10.2174/156802611795165098

[26]   Korhonova, M., Doricakova, A., & Dvorak, Z. (2015). Optical Isomers of Atorvastatin, Rosuvastatin and Fluvastatin Enantiospecifically Activate Pregnane X Receptor PXR and Induce CYP2A6, CYP2B6 and CYP3A4 in Human Hepatocytes. *Plos One*, *10*(9). doi: 10.1371/journal.pone.0137720

[27]   Greenberg, W. A., Varvak, A., Hanson, S. R., Wong, K., Huang, H., Chen, P., & Burk, M. J. (2004). Asymmetric Catalysis Special Feature Part II: Development of an efficient, scalable, aldolase-catalyzed process for enantioselective synthesis of statin intermediates. *Proceedings of the National Academy of Sciences*, *101*(16), 5788–5793. doi: 10.1073/pnas.0307563101

[28]   Windle, C. L., Müller, M., Nelson, A., & Berry, A. (2014). Engineering aldolases as biocatalysts. *Current Opinion in Chemical Biology*, *19*, 25–33. doi: 10.1016/j.cbpa.2013.12.010

[29]   Müller, M. (2012). Recent Developments in Enzymatic Asymmetric C-C Bond Formation. *Advanced Synthesis & Catalysis*, *354*(17), 3161–3174. doi: 10.1002/adsc.201100655

[30]   Watson, D. G. (2011). *Pharmaceutical chemistry*. Edinburgh: Churchill Livingstone

[31]   Suzuki, A. (2005). Carbon–carbon bonding made easy. *Chemical Communications*, (38), 4759. doi: 10.1039/b507375h

[32] M. Haridas, E. M. M. Abdelraheem, and U. Hanefeld, "2-Deoxy-d-ribose-5-phosphate aldolase (DERA): applications and modifications," *Appl. Microbiol. Biotechnol.*, vol. 102, no. 23, pp. 9959–9971, 2018.

[33] Dean, S. M., Greenberg, W. A., & Wong, C.-H. (2007). Recent Advances in Aldolase-Catalyzed Asymmetric Synthesis. *Advanced Synthesis & Catalysis*, *349*(8-9), 1308–1320. doi: 10.1002/adsc.200700115

[34] Sheldon, R. A., Arends, I. W. C. E., & Hanefeld, U. (2008). *Green chemistry and catalysis*. Weinheim: Wiley-VCH

[35] Nature Education. (n.d.). *Enzymes*. *Principles of Biology*. Retrieved from https://dls.ym.edu.tw/course/hb/doc/lecture4-(11) 11-Enzymes.pdf

[36] Robinson, P. K. (2015). Enzymes: principles and biotechnological applications. *Essays In Biochemistry*, *59*(0), 1–41. doi: 10.1042/bse0590001

[37] Milner, S. E., & Maguire, A. R. (2012). Recent trends in whole cell and isolated enzymes in enantioselective synthesis. *Arkivoc*, *2012*(1), 321–382. doi: 10.3998/ark.5550190.0013.109

[38] Carvalho, C. C. C. R. de, & Fonseca, M. R. da. (2007). Bacterial Whole Cell Biotransformations: In Vivo Reactions Under In Vitro Conditions. *Dynamic Biochemistry, Process Biotechnology and Molecular Biology*, *1*(1), 32–39

[39] Ma, S. K., Gruber, J., Davis, C., Newman, L., Gray, D., Wang, A., … Sheldon, R. A. (2010). A green-by-design biocatalytic process for atorvastatin intermediate. *Green Chem.*, *12*(1), 81–86. doi: 10.1039/b919115c

[40] Wong, C.-H., Garcia-Junceda, E., Chen, L., Blanco, O., Gijsen, H. J. M., & Steensma, D. H. (1995). Recombinant 2-Deoxyribose-5-phosphate Aldolase in Organic Synthesis: Use of Sequential Two-Substrate and Three-Substrate Aldol Reactions. *Journal of the American Chemical Society*, *117*(12), 3333–3339. doi: 10.1021/ja00117a003

[41] Faber, K., Fessner, W.-D., & Turner, N. J. (2015). *Biocatalysis in organic synthesis*. Stuttgart: Georg Thieme Verlag

[42] Samland, A. K., & Sprenger, G. A. (2006). Microbial aldolases as C–C bonding enzymes—unknown treasures and new developments. *Applied Microbiology and Biotechnology*, *71*(3), 253–264. doi: 10.1007/s00253-006-0422-6

[43] Schulte, M., Petrović, D., Neudecker, P., Hartmann, R., Pietruszka, J., Willbold, S., … Panwalkar, V. (2018). Conformational Sampling of the Intrinsically Disordered C-Terminal Tail of DERA Is Important for Enzyme Catalysis. *ACS Catalysis*, *8*(5), 3971–3984. doi: 10.1021/acscatal.7b04408

[44] Heine, A., Luz, J. G., Wong, C.-H., & Wilson, I. A. (2004). Analysis of the Class I Aldolase Binding Site Architecture Based on the Crystal Structure of 2-Deoxyribose-5-phosphate Aldolase at 0.99Å Resolution. *Journal of Molecular Biology*, *343*(4), 1019–1034. doi: 10.1016/j.jmb.2004.08.066

[45] Heine, A., Desantis, G., Luz, J., Mitchell, M., Wong, C.-H., & Wilson, I. (2001). Observation Of Covalent Intermediates In An Enzyme Mechanism At Atomic Resolution. *Science*, *294*, 369–374. doi: 10.2210/pdb1jcl/pdb

[46] Wierenga, R. (2001). The TIM-barrel fold: a versatile framework for efficient enzymes. *FEBS Letters*, *492*(3), 193–198. doi: 10.1016/s0014-5793(01)02236-0

[47] Desantis, G., Liu, J., Clark, D. P., Heine, A., Wilson, I. A., & Wong, C.-H. (2003). Structure-Based mutagenesis approaches toward expanding the substrate specificity of d-2-Deoxyribose-5-phosphate aldolase. *Bioorganic & Medicinal Chemistry*, *11*(1), 43–52. doi: 10.1016/s0968-0896(02)00429-7

[48] Dick, M., Hartmann, R., Weiergräber, O. H., Bisterfeld, C., Classen, T., Schwarten, M., … Pietruszka, J. (2016). Mechanism-based inhibition of an aldolase at high concentrations of its natural substrate acetaldehyde: structural insights and protective strategies. *Chemical Science*, *7*(7), 4492–4502. doi: 10.1039/c5sc04574f

[49] Ručigaj, A., & Krajnc, M. (2013). Optimization of a Crude Deoxyribose-5-phosphate Aldolase Lyzate-Catalyzed Process in Synthesis of Statin Intermediates. *Organic Process Research & Development*, *17*(5), 854–862. doi: 10.1021/op400040b

[50]   Vajdič, T., Ošlaj, M., Kopitar, G., & Mrak, P. (2014). Engineered, highly productive biosynthesis of artificial, lactonized statin side-chain building blocks: The hidden potential of Escherichia coli unleashed. *Metabolic Engineering*, *24*, 160–172. doi: 10.1016/j.ymben.2014.05.012

[51]   Jennewein, S., Schürmann, M., Wolberg, M., Hilker, I., Luiten, R., Wubbolts, M., & Mink, D. (2006). Directed evolution of an industrial biocatalyst: 2-deoxy-D-ribose 5-phosphate aldolase. *Biotechnology Journal*, *1*(5), 537–548. doi: 10.1002/biot.200600020

[52]   Ručigaj, A., & Krajnc, M. (2015). Kinetic modeling of a crude DERA lysate-catalyzed process in synthesis of statin intermediates. *Chemical Engineering Journal*, *259*, 11–24. doi: 10.1016/j.cej.2014.07.124

[53]   Klotzbuecher , P. (2015). *cGMP and Regulatory Considerations of Continuous Manufacturing Processes. 2nd FDA/PQRI Conference on Advancing Product Quality*. Retrieved May 20, 2019, from http://pqri.org/wp-content/uploads/2015/09/03-Klotzbuecher_RegulatoryCM_29SEP2015.pdf

[54]   Wiles, C., & Watts, P. (2012). Continuous flow reactors: a perspective. *Green Chem.*, *14*(1), 38–54. doi: 10.1039/c1gc16022b

[55]   Gutmann, B., Cantillo, D., & Kappe, C. O. (2015). Continuous-Flow Technology-A Tool for the Safe Manufacturing of Active Pharmaceutical Ingredients. *Angewandte Chemie International Edition*, *54*(23), 6688–6728. doi: 10.1002/anie.201409318

[56]   Poechlauer, P., Manley, J., Broxterman, R., Gregertsen, B., & Ridemark, M. (2012). Continuous Processing in the Manufacture of Active Pharmaceutical Ingredients and Finished Dosage Forms: An Industry Perspective. *Organic Process Research & Development*, *16*(10), 1586–1590. doi: 10.1021/op300159y

[57]   May, S. A. (2017). Flow chemistry, continuous processing, and continuous manufacturing: A pharmaceutical perspective. *Journal of Flow Chemistry*, *7*(3–4), 137–145. doi: 10.1556/1846.2017.00029

[58]   Jiménez-González, C., Poechlauer, P., Broxterman, Q. B., Yang, B.-S., Ende, D. A., Baird, J., … Manley, J. (2011). Key Green Engineering Research Areas for Sustainable Manufacturing: A Perspective from Pharmaceutical and Fine Chemicals Manufacturers. *Organic Process Research & Development*, *15*(4), 900–911. doi: 10.1021/op100327d

[59]   Gottlieb, S., Woodcock, J. (2019, February 26). FDA statement on FDA's modern approach to advanced pharmaceutical manufacturing. Retrieved from https://www.fda.gov/news-events/press-announcements/fda-statement-fdas-modern-approach-advanced-pharmaceutical-manufacturing?platform=hootsuite

[60]   Center for Drug Evaluation and Research. (n.d.). Quality Considerations for Continuous Manufacturing. Retrieved from https://www.fda.gov/regulatory-information/search-fda-guidance-documents/quality-considerations-continuous-manufacturing

[61]   FDA Approved Drugs. (n.d.). Retrieved May 20, 2019, from https://www.centerwatch.com/drug-information/fda-approved-drugs/

[62]   Levenspiel, O. (2012). *Tracer technology: modeling the flow of fluids*. New York: Springer

[63]   Levenspiel, O. (1999). *Chemical reaction engineering* (3rd ed.). New York: Wiley

[64]   Dwevedi, A. (2016). Basics of Enzyme Immobilization. *Enzyme Immobilization*, 21–44. doi: 10.1007/978-3-319-41418-8_2

[65]   Phisalaphong, M., Budiraharjo, R., Bangrak, P., Mongkolkajit, J., & Limtong, S. (2007). Alginate-loofa as carrier matrix for ethanol production. *Journal of Bioscience and Bioengineering*, *104*(3), 214–217. doi: 10.1263/jbb.104.214

[66]   Lee, K. Y., & Mooney, D. J. (2012). Alginate: properties and biomedical applications. *Progress in Polymer Science*, *37*(1), 106–126. doi: 10.1016/j.progpolymsci.2011.06.003

[67]   Kobašlija, M., & Mcquade, D. T. (2006). Removable Colored Coatings Based on Calcium Alginate Hydrogels. *Biomacromolecules*, *7*(8), 2357–2361. doi: 10.1021/bm060341q

[68]   Ogbonna, J. C., Liu, Y.-C., Liu, Y.-K., & Tanaka, H. (1994). Loofa (Luffa cylindrica) Sponge as a Carrier for Microbial Cell Immobilization. *Journal of Fermentation and Bioengineering*, *78*(6), 437–442

[69]   Shen, J., Xie, Y. M., Huang, X., Zhou, S., & Ruan, D. (2012). Mechanical properties of luffa sponge. *Journal of the Mechanical Behavior of Biomedical Materials*, *15*, 141–152. doi: 10.1016/j.jmbbm.2012.07.004

[70]   Lee, B.-B., Ravindra, P., & Chan, E.-S. (2013). Size and Shape of Calcium Alginate Beads Produced by Extrusion Dripping. *Chemical Engineering & Technology*, *36*(10), 1627–1642. doi: 10.1002/ceat.201300230

[71] Pignolet, L. H., Waldman, A. S., Schechinger, L., Govindarajoo, G., & Nowick, J. S. (n.d.)

[72] Ošlaj, M., Cluzeau, J., Orkić, D., Kopitar, G., Mrak, P., & Časar, Z. (2013). A Highly Productive, Whole-Cell DERA Chemoenzymatic Process for Production of Key Lactonized Side-Chain Intermediates in Statin Synthesis. *PLoS ONE*, *8*(5). doi: 10.1371/journal.pone.0062250

[73] Fesko, K., & Gruber-Khadjawi, M. (2013). Biocatalytic Methods for C-C Bond Formation. *ChemCatChem*, *5*(6), 1248–1272. doi: 10.1002/cctc.201200709

[74] Hazardous Substances Data Bank (HSDB). (n.d.). Retrieved June 15, 2019, from https://toxnet.nlm.nih.gov/cgi-bin/sis/search2/r?dbs+hsdb:@term+@rn+@rel+100-52-7

[75] Hazardous Substances Data Bank (HSDB). (n.d.). Retrieved June 15, 2019, from https://toxnet.nlm.nih.gov/cgi-bin/sis/search2/r?dbs+hsdb:@term+@rn+@rel+104-55-2

[76] Pérez, J. M., Arenas, F. A., Pradenas, G. A., Sandoval, J. M., & Vásquez, C. C. (2008). Escherichia coliYqhD Exhibits Aldehyde Reductase Activity and Protects from the Harmful Effect of Lipid Peroxidation-derived Aldehydes. *Journal of Biological Chemistry*, *283*(12), 7346–7353. doi: 10.1074/jbc.m708846200

[77] Lee, C., Kim, I., Lee, J., Lee, K.-L., Min, B., & Park, C. (2010). Transcriptional Activation of the Aldehyde Reductase YqhD by YqhC and Its Implication in Glyoxal Metabolism of Escherichia coli K-12. *Journal of Bacteriology*, *192*(16), 4205–4214. doi: 10.1128/jb.01127-09

[78] Bramski, J., Dick, M., Pietruszka, J., & Classen, T. (2017). Probing the acetaldehyde-sensitivity of 2-deoxy-ribose-5-phosphate aldolase (DERA) leads to resistant variants. *Journal of Biotechnology*, *258*, 56–58. doi: 10.1016/j.jbiotec.2017.03.024

[79] Cao, T.-P., Kim, J.-S., Woo, M.-H., Choi, J. M., Jun, Y., Lee, K. H., & Lee, S. H. (2016). Structural insight for substrate tolerance to 2-deoxyribose-5-phosphate aldolase from the pathogen Streptococcus suis. *Journal of Microbiology*, *54*(4), 311–321. doi: 10.1007/s12275-016-6029-4

[80] Fogler, H. S. (2006). *Elements of chemical reaction engineering*. Upper Saddle River, NJ: Prentice Hall PTR/Pearson Education

[81] Stolarzewicz, I. A. (2017). Study on the Properties of Immobilized Biocatalysts with Lipase Activity Produced by Yarrowia lipolytica in Batch Culture. *Chemical and Biochemical Engineering Quarterly*, *31*(3), 251–259. doi: 10.15255/cabeq.2016.833

[82] Chaplin, M. (n.d.). Enzyme Technology: Packed bed reactors. Retrieved July 1, 2019, from http://www1.lsbu.ac.uk/water/enztech/pbr.html

[83] Lichtenegger, G. J., Tursic, V., Kitzler, H., Obermaier, K., Khinast, J. G., & Gruber-Wölfler, H. (2016). The Plug & Play Reactor: A Highly Flexible Device for Heterogeneous Reactions in Continuous Flow. *Chemie Ingenieur Technik*, *88*(10), 1518–1523. doi: 10.1002/cite.201600013

[84] Lotfipour, F., Mirzaeei, S., & Maghsoodi, M. (2012). Evaluation of the effect of CaCl2 and alginate concentrations and hardening time on the characteristics of Lactobacillus acidophilus loaded alginate beads using response surface analysis. *Advanced Pharmaceutical Bulletin*, *2*(1), 71–78. doi: 10.5681/apb.2012.010

[85] Blandino , A., Macias, M., & Cantero, D. (1999). Formation of Calcium Alginate Gel Capsules: Influence of Sodium Alginate and CaC12 Concentration on Gelation Kinetics. *Journal of Bioscience and Bioengineering*, *88*(6), 686–689

[86] Russo, R., Malinconico, M., & Santagata, G. (2007). Effect of Cross-Linking with Calcium Ions on the Physical Properties of Alginate Films. *Biomacromolecules*, *8*(10), 3193–3197. doi: 10.1021/bm700565h

[87] Takka, S., & Gürel, A. (2010). Evaluation of Chitosan/Alginate Beads Using Experimental Design: Formulation and In Vitro Characterization. *AAPS PharmSciTech*, *11*(1), 460–466. doi: 10.1208/s12249-010-9406-z

[88] Taqieddin, E., & Amiji, M. (2004). Enzyme immobilization in novel alginate–chitosan core-shell microcapsules. *Biomaterials*, *25*, 1937–1945. doi: 10.1016/j.biomaterials.2003.08.034
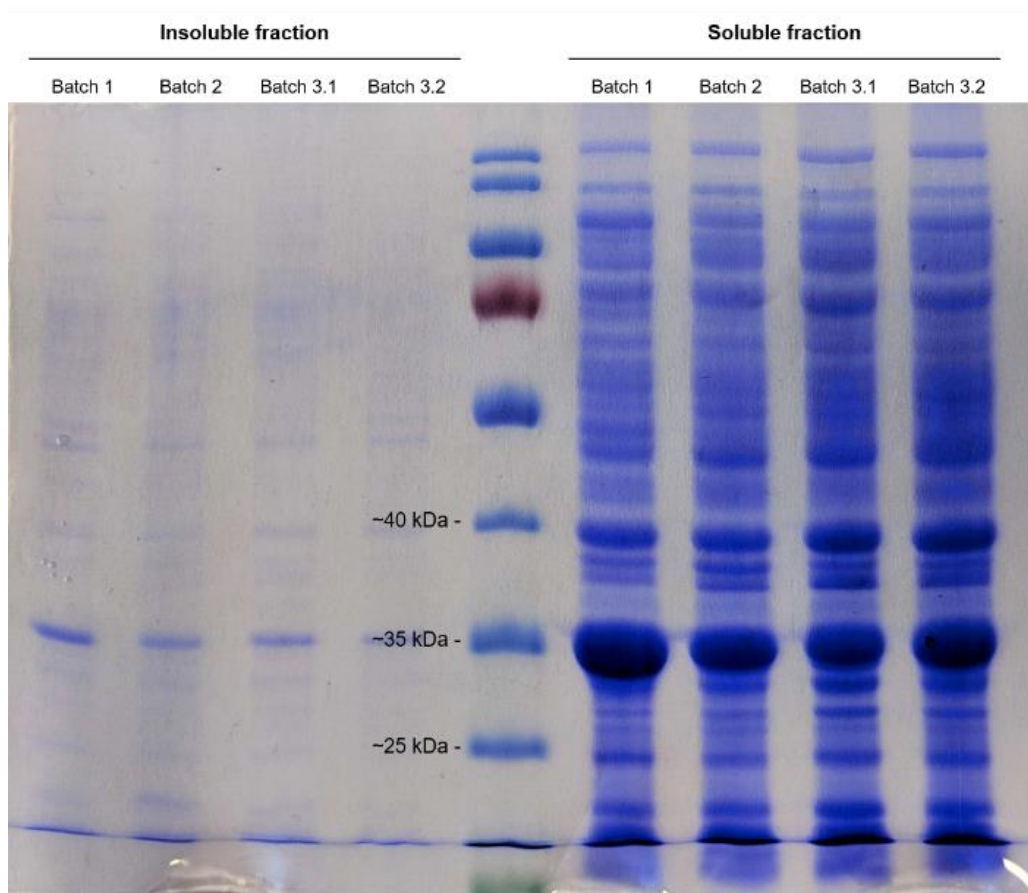
7 Appendix

Figure 7.1: SDS-PAGE of freeze-dried E. coli BL21 (DE3), containing overexpressed DERA (27.7 kDa).